Optimizing Charging Schedules for Electrified Aircraft at RTHA Airport

Balancing Cost and Time for Electric Aviation

Master Thesis

Raf van de Luijtgaarden

Delft University of Technology

TU Delft

Optimizing Charging Schedules for Electrified Aircraft at RTHA Airport

Balancing Cost and Time for Electric Aviation

by

Raf van de Luijtgaarden

Master of Science in Electrical Engineering
DC Systems, Energy Conversion & Storage

Thesis Committee and Guidance:

Chair:	Dr. J. Dong
Core Member:	Dr. O.A. Sharpans'kykh
Supervisor:	Prof.dr.ir. P. Bauer
Daily Supervisor:	Dr. G.R. Chandra Mouli
Daily co-supervisor:	Y. Liang
Faculty:	Electrical Engineering, Mathematics and Computer Science, Delft

To be defended in public on 11/07/2025

TU Delft

Abstract

This thesis develops a mathematical optimization model to optimize charging schedules and energy management for electrified aircraft at Rotterdam The Hague Airport (RTHA), addressing research gaps in adapting airport infrastructure for electric aviation. Based on a real-life flight schedule from 2019, the model determines a Battery Energy Storage System (BESS) size while minimizing operational costs, such as grid electricity, photovoltaic (PV) use, BESS degradation, and flight delay/cancellation penalties, while trying to maintain the schedule as closely as possible. Five electric aircraft types, ranging from a 2-seater flight school aircraft, to a 90-seater commercial aviation model, were considered with a Constant Power - Constant Voltage (CPCV) charging profile, alongside a detailed mission energy analysis. Seasonal simulation for January, April, July, and October 2019 showed delays averaging from 2 minutes in July while peaking at 45 in January, alongside three flight cancellations due to high energy demands. Optimized BESS sizes range from 7 MWh to 12 MWh. Optimization of the model showed a reduction of up to €500,000 weekly when compared to a baseline case. Sensitivity analysis showed that increasing the grid import limits from 3.5 MW to 5 MW gave better grid reliability, with less delays and cancellations, while a decrease to 2 MW showed increases in delay times and cancellations. When the export limit was reduced from 7.5 MW to 5 MW, the delays increased due to constrained energy offloading, while increasing it to 10 MW decreased the delays and cancellations by one. A 1 MWh BESS increase reduced cancellations by one and total delay time by up to 5 hours. Adjusting the turnaround times by $\pm$ 15 minutes demonstrated the model's resilience to stricter turnaround times, but a 4-hour delay increase was present with extensions. The findings of the thesis show the critical role that BESS capacity and grid limits play in ensuring operational efficiency for the electric aviation infrastructures of the future, but also the cost and delay reduction by optimizing charging schedules.

Foreword

When starting this Master program, I had no idea that the thesis I would write would again be on the topic electric aviation, just like in my Bachelor thesis. Seeing the possibility to dig deeper into the workings of an airport, while optimizing certain aspects for the future of electric aviation, it felt like I came full circle. In the last 9 months, I learned a lot about airport operations, programming, and energy systems. The latter being one of my favorite aspects of the education that I have gotten in the last few years in Delft.

This thesis would not have been possible without the help of several people. First of all, I would like to thank Gautham Ram for providing me with the opportunity to tackle this problem as part of my thesis and giving me guidance about optimization problems. I also want to thank the people from Rotterdam The Hague Airport for providing me with the needed data for the model, as well as giving me the opportunity to give a presentation in the *Future Energy Cafe* about this thesis. Additionally, I would like to thank Dr. Alexei Sharpans'kykh from Aerospace Engineering, and Joost Commandeur from Shell for their incredibly valuable feedback and insight into aspects in the thesis I did not yet consider. Last, but most importantly, I want to extend my greatest thanks to Yawen Liang, for guiding me on a day-to-day basis, discussing ideas, and helping me find my footing during the duration of the thesis. Her help was beneficial to this project and I have learned a lot from her in the last few months.

Finally, I want to thank my family and friends for their support during my studies and this thesis. I want to give a special thanks to my parents William and Aleksandra, for providing me with the opportunity to study at TU Delft, and my sister Adasia for their never-ending support, love, and belief in me.

Raf van de Luijtgaarden
Delft, June 2025

Contents

1 Introduction

1.1. Background and Motivation

Over the recent years, the aviation sector has faced increasing pressure to reduce its carbon footprint. In addition to sustainable aviation fuel, electric aircraft (EA) are seen as part of the solution to achieve a net zero future of flying.

EUROCONTROL predicts that by 2050, almost 10% of flights will be hybrid or fully electric [1]. Airports, as key players in the aviation network, must adapt to support these types of aircraft while maintaining operational efficiency. Larger electric aircraft, designed for short- to medium-haul commercial routes, like the 90-seater Elysian, are increasingly feasible and might be closer to reality than previously thought [2]. However, their high energy demands and tight turnaround times at airports pose challenges to power management and operational feasibility. Rotterdam the Hague Airport (RTHA), a regional airport in the Netherlands, is acknowledging the need for a change in infrastructure to support these aircraft. Optimizing infrastructure and charging schedules is an essential step towards balancing the load on the electricity network and making sure that every flight is charged while minimizing delays in the flight schedule.

Although recent studies on electric aircraft technology have shown that their future is brighter than anticipated, there is still a lack of studies that address how airports can prepare and optimize their infrastructure to accommodate the increase in electric flights, particularly for commercial purposes involving a range of electric aircraft.

This thesis addresses this challenge by developing a framework that can optimize the infrastructure and charging schedules at RTHA, which aligns the operations of multiple short- to medium-haul electric aircraft with real-life flight schedules.

1.2. Research Gap

Current approaches to the topic of electric aviation or its adaptation into real-world scenarios vary wildly. However, when analyzing the research that has been done, it becomes clear that there are still gaps in the knowledge or execution of the work. In this subsection, several other studies regarding the topic of electric aviation and its infrastructure will be briefly summarized and their research gaps identified.

Hou et al. [3] studies the impact that Hybrid Electric Aircraft (HEA) would have on airport operations. Here, they make several assumptions to calculate the energy needs for these aircraft as well as their distance. With this, they propose changes to the flight schedule that reduce peak power demand, which in turn lowers the need for infrastructure upgrades. These changes can be made by the airport, or by the airlines themselves. Lastly, they consider larger airports in their case study, such as the John F. Kennedy International Airport in New York, moving away from the smaller, regional airports. Here, they

found that strategic rescheduling of flights can reduce power peaks by upwards of 50%.

Mitici, Pereira and Oliviero [4] aims to propose a flight schedule for small and large electric aircraft that uses normal battery charging and delves into the concept of battery-swapping. Battery swapping is a tactic that allows an airplane to physically swap its depleted battery with a fresh, full battery that is stored at an airport. This minimizes the turnaround time that would normally limit the airport operations. They take into account the acquisition cost of a fleet of EA, the charging stations, and the swap batteries. In their model they assume time constants for the swapping of the battery and the loading/unloading of the passengers. A bi-linear charging profile is used, where the battery is charged with a high power during the first 90% of the State of Charge (SoC), and then changes to a lower power to finish the last 10% to minimize degradation of the battery cells. The energy expenditure of the aircraft is determined linearly and a reserve of 20% is taken into account. In the objective, they also consider the operational cost of charging these aircraft, together with a large penalty if a certain flight mission is not fulfilled.

In Patrik Ollas et al. [5], the role of solar systems and battery storage systems (BESS) in supporting short-haul electric aviation and electric vehicle (EV) infrastructure at Visby airport in Sweden is evaluated. They consider technical and economical analysis to model PV installations at several locations around to airport, together with an optimization to size a BESS to manage the increase energy demands from EA and EVs. They optimize the system for self-consumption, where the energy from renewables and the battery system is maximized for their own use. With this, peaks can be reduced by 6-7 MW. Additionally, they use a battery degradation model that models the capacity loss in batteries due to usage. However, because Visby is a small regional airport, only small aircraft with a limited range of 200 km are taken into account.

The thesis by A. Laurell [6] investigates the charging infrastructure needed to support EA at an arbitrary airport, where the focus is on the power demands and the role of a BESS and a PV system. Here, a model was constructed to simulate the operations of an airport, such as the charging of the aircraft and the power demands of the whole system. The study was conducted to address grid capacity challenges in Sweden, where the addition of EA in airports introduces high peak demands due to low turnaround times at airports. Several scenarios were conducted with varying charger amounts, BESS capacities, BESS power ratings and a 7000 m^2 PV plant during the month of June. The study found that a BESS significantly reduces the peaks, and that the PV system compliments the BESS by recharging it during the middays, where the sun is at its peaks. Here, one type of EA was taken into account, with a battery size of 750 kWh, and a charging strategy that lowers power when getting close to a fully charged EA battery. However, the study also makes assumptions about battery specifications, charging technology, and arrival data.

In Vehlhaber and Salazar [7], an optimization of EA operations to minimize grid dependency on the remote Dutch Antilles islands of Aruba, Bonaire and Curaçao by utilizing renewable energy. It focuses on short-haul routes and takes into account fleet assignment, flight routes, and charging schedules, all while considering PV systems and BESS implementations at the airports. For these flights, a 9-seater EA called Alice is assumed, together with a 2000 m^2 PV installation and a 1 MWh BESS. The optimized schedule reduces grid energy by 20-100% depending on the weather conditions. In the future, a high potential for grid independence is shown for these island airports, even with simplified energy models and assuming the airport only consumes power, and doesn't feed it back.

The paper by van Oosterom and Mitici [8] looks into the optimization of battery charging and swapping for short-haul EA for Widerøe Airlines in Norway. They aim to determine the optimal charging power and amount of spare batteries needed at several hub airports across Norway to support battery swapping. Additionally, a minimalization problem is written for infrastructure, electricity, operation, and flight delays costs. First, the optimizer is used to calculate the needed charging capacity, together with the amount of spare batteries. Afterwards, the optimizer looks for the best strategy to charge the EA batteries. For these flights, the 9-seater EA Alice is assumed once more. Limitations of the paper include a fixed flight schedule with no delays or cancellations, only a single aircraft type, and reduced capacity needing extra flights.

Lastly, in Meindl et al. [9], an infrastructure expansion for the Albrecht Dürer Airport Nürnberg in Germany to support HEA is studied. Using data from both the Nürnberg Airport and RTHA, it studies the inclusion of PV systems, wind power and a BESS to meet increased demands at the airport while optimizing for cost and low emissions. A 50 seater HEA model with a battery size of 840 kWh is used and can replace up to 6,100 flight annually. A PV system was constructed in the simulation of 14 MW_p together with a 3 MW wind turbine to reduce the electricity cost by up to 3 million euro's annually. This, together with a 4 MWh BESS can support the HEA implementation at the airport. The BESS uses a degradation model and it is estimated that the aging loss is between 6-15% after 3 years of use.

After reviewing previous work on electric aviation and its impact on infrastructure and airports, certain gaps can be found. A large number of studies utilize rescheduling techniques such as altering flights schedules and imposing large penalties when a flight is not sufficiently charged. This is particularly relevant for electric aircraft, where the turnaround times and power peaks pose as substantial challenges. However, these studies often focus on rescheduling flights altogether or single penalties, leaving an unexplored gap of using delays and cancellation strategies to manage operations. This research addresses this gap by optimizing electric aviation scheduling with flexible delays and selective cancellations, removing the need to swap flights altogether and minimizing costs. Additionally, it offers a greater adaptation to the real-life flight schedule instead of creating a new one from scratch.
Then, several studies look at the implementation of a BESS and a PV park to aid the system in delivering power. However, they do not iteratively solve for an optimal BESS size or PV park, or they do not take the aging of the BESS into account when modeling the system.
For the charging profile, none or simple profiles are chose to deliver the energy to the EA battery. In most cases, high power charging is allowed until a certain threshold, and then the power is lowered linearly in the latter stages of charging. In real life, many charging profiles follow a Constant Current - Constant Voltage (CCCV) profile, or a Constant Power - Constant Voltage (CPCV) profile that take the cell characteristics into account, and are based on non-linear modeling.
In terms of the aircraft used, many studies focus on one or at best, two types of electric aircraft. In the case where commercial aviation is considered, the aircraft are all hybrid EA, where the batteries are smaller than that of a fully electric commercial aircraft, lowering the amount of power needed to charge these aircraft.
Finally, when the energy needs of the aircraft during the mission are considered, a simple, linear approximation of energy use is chosen in previous studies. However, during its mission, an aircraft will go through multiple flight stages, such as take-off, climbing, and cruising. These stages require different powers from the aircraft and could be a better way to model the energy needs of an electric aircraft's flight.

In Table 1.1, an overview of the summarized studies can be found and if they consider one of the goals that were found during the literature review.

Table 1.1: Summary of Related Studies

	Schedule Changes	**Optimal BESS Sizing**	**Commercial Aviation**	**CPCV**	**BESS Degradation**	**Accurate Mission Energy**
[3]	✓	✖	✓	✖	✖	✖
[4]	✓	✖	✓	✖	✖	✖
[5]	✖	✓	✖	✖	✓	✖
[6]	✓	✓	✖	✖	✖	✖
[7]	✖	✓	✖	✖	✖	✖
[8]	✓	✖	✓	✖	✖	✖
[9]	✓	✖	✓	✖	✓	✖
This study	✓	✓	✓	✓	✓	✓

1.3. Research Goal

With the research gap in mind, the goal of the thesis can now be determined. In this paper, the goal is to write an *optimization problem* that, based on a real-life flight schedule at RTHA, can determine an appropriate BESS size to aid the operations of the airport for electric aviation to keep the flight schedule as close as possible to one used in the present day while also minimizing cost of investment and operations. Here, five types of electric aircraft with different passenger capacities and ranges will be considered, together with a CPCV charging profile to charge the aircraft, a BESS degradation model and, most importantly, fully electric commercial aircraft will now be considered alongside smaller electric aircraft, with a detailed analysis of their energy needs during a mission. With these assumptions in mind, the optimizer will have the objective of minimizing the cost of operations, including grid electricity costs, PV, BESS degradation, and potential flight delay/cancellation costs.

How can the charging schedule for multiple types of electric aircraft at RTHA be optimized to minimize operational costs while adhering to a real-life flight schedule?

2

Data Analysis and Preparation

Before the optimization can be written, the required input data needs to be prepared. This chapter delves into the different inputs, how they were obtained, and how they were prepared for the optimization application.

2.1. Data Overview

For an optimization, data is key. In the case of RTHA, several datasets have been provided.
Firstly, the flight schedule. RTHA provided the project with an actual, full flight schedule from 2019. Based on the schedule, the workings of the airport and its flights are studied, and allows research to be done in regards of which aircraft can be replaced with an electric one.
The airport is equipped with a PV park rated for 13 MW_p located next to the runway. At the time of writing this thesis, the park is being leased to surrounding parties. However, RTHA stated in communication that the future plan is to use the PV park themselves again. Therefore, the PV data will be included in the optimization.
Next, information regarding the demand at the airport itself is needed. This includes lighting, powering shops, equipment, etc. and should be determined.
Lastly, energy pricing for the year 2019 needs to be acquired to help the optimizer calculate the price for electricity, based on real-life values.

Assumptions

For this research, several assumptions regarding the system, data inputs, and energy expenditures are made. Below, these assumptions are listed.

- Mission energy per flight is based off the optimal route and on full capacity, flying straight from A to B, without deviations, while still accounting for reserves.
- Mission energy per flight does not take weather and seasonal variations into account which may cause the energy requirement to fluctuate. This is beyond the scope of this thesis.
- The only variable in mission energy per flight is the cruising time, which has been set to the flown distance to simplify calculations.
- A flight is eligible for electrification based on range, not on passenger throughput as current electric aircraft technology is limited to lower capacities. The split between 1st and 2nd generation electric commercial aviation is based on the original aircraft's passenger capacity of 123 PAX. Below 123 PAX is 1st generation, above is for 2nd generation, working in tandem with the range specifications.
- All data inputs are from 2019, except the airport's energy demand, which is from 2023. The data from 2023 should be reasonable to use alongside the 2019 data, as ground energy demand data is less volatile from year to year.

- Efficiencies of cables, converters, transformers, etc. is set to 100% to simplify the model.
- Each airport that aircraft fly to has the infrastructure to charge the aircraft.
- The charge and discharge C-rates of the BESS are higher than those of standard large-scale BESS installations which range between 0.25C-1C [10]. They are set to a maximum of 2C, which assumes advancements in battery technology in the future.
- The lowest BESS cost per kWh is taken to account for advancements. This cost is not being optimized and can be multiplied by other prices after simulation.
- Taxi time and plug-in time for the aircraft is not taken into account to maximize turnaround times that can be used for charging purposes.

2.2. Data Preparation

In the following sections the datasets for the simulation will be discussed. First, we will discuss the three least intensive datasets, namely the PV power data, the airport power demand, and lastly the electricity price. Then, the flight schedule will be broken down in detail and prepared for the final optimization.

2.2.1. PV

To let the model know exactly how much PV power is available, and at which timestep, the PHOTOVOLTAIC GEOGRAPHICAL INFORMATION SYSTEM (PVGIS) website of the European Commission is used [11]. Here, historical data on weather and PV systems can be analyzed. In Figure 2.1, a snippet of the website can be seen. Here, one can select the year for which the data is needed, the location of the PV system, the solar irradiation database, the technology used in the solar panels, the installed peak power (13 MW in this case), the losses, which by default are 14%, which is kept, and lastly the mounting position of the panels, which can be optimized on the website as they are unknown.

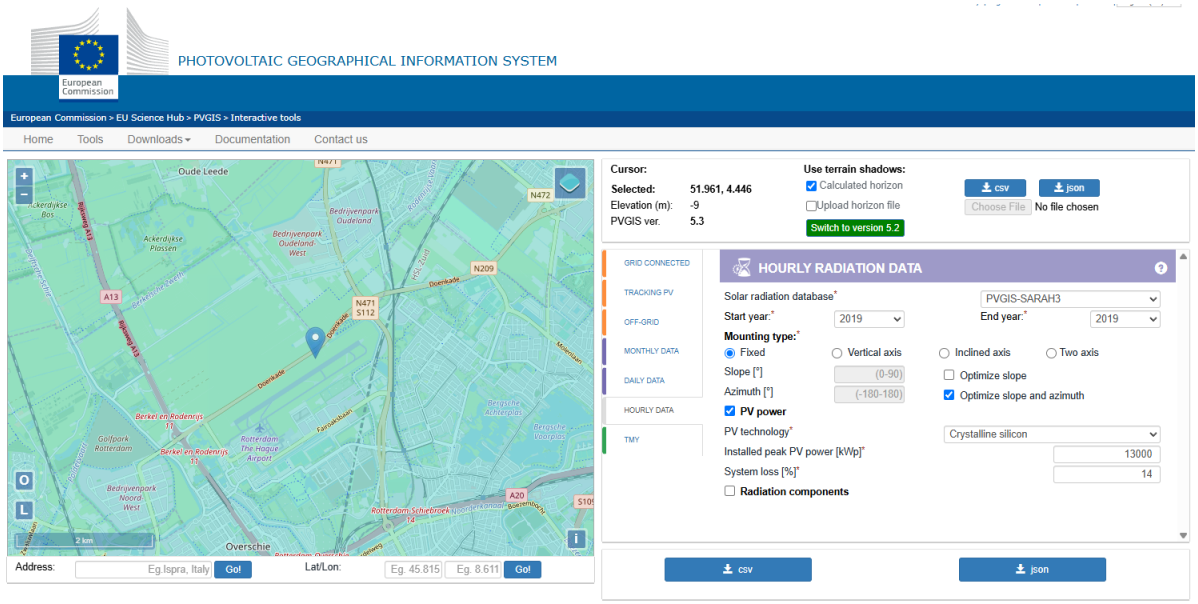

Figure 2.1: PVGIS Website Functionality and Settings

After entering the necessary information on the website, a Comma Separated Values (CSV) file is downloaded. Only the two columns that contain information about the power and date are obtained. However, the time intervals originally used are measured in hours. To ensure granularity and viability, 15-minute intervals will be used in the project.
The original time intervals are in 1-hour which are transformed to 15-minutes to ensure consistent time intervals in the thesis. Lastly, the PV power is divided by 1000 to set the values to kW instead of W.
Table 2.1 shows a snippet of the original CSV and one of the final PV power CSV that is used in the optimization.

Table 2.1: Snippet of original PV CSV and final PV power CSV

time	P (W)
20190101:0711	0
20190101:08711	0
20190101:0911	201500
20190101:1011	290030

time	P (kW)
01/01/2019 08:15:00	0
01/01/2019 08:30:00	50.37
01/01/2019 08:45:00	100.75
01/01/2019 09:00:00	151.125

2.2.2. Airport Demand

Another key part of information that should be known for the optimizer is the power demand of the airport. With this, the solver will know how much power has to be delivered to the airport at which time and how much can be delegated for the charging of the aircraft. The airport demands mainly consist of lighting, air conditioning, appliances used, etc.
The energy and power usage of the chosen airport was provided by RTHA. In this CSV, the timestep is already in 15-minute intervals, and mentions how much energy is consumed by the airport at that time in kWh. The date is change to 2019 to match PV and flight schedule data, with the same 15-minute intervals. Energy and power are related by Equation 2.1, and by moving the time factor to the energy side, the power can be calculated. Since 15 minutes is $\frac{1}{4}$ of an hour, the energy is multiplied by a factor of 4 to determine the power use of that interval.

$$E = P \cdot t \tag{2.1}$$

Finally, another snippet of the final CSV can be seen in Table 2.2

Table 2.2: Snippet of final airport demand CSV.

time	P (kW)
01/01/2019 08:15:00	529.44
01/01/2019 08:30:00	486.47
01/01/2019 08:45:00	485.95
01/01/2019 09:00:00	502.05

2.2.3. Electricity Price

The final piece before moving to the flight schedule is the market price for electricity in 2019. This price for 2019 comes from the *European Network of Transmission System Operators for Electricity* (ENTSO-E) [12]. On their website, historical data on electricity pricing can be found. Here, the data is provided in 1-hour intervals, with a price associated to it in €/MWh [13]. Using Pandas, these times are changed to the desired 15-minute intervals, and the prices are divided by a factor of 1000 to know the pricing in €/kWh. In Figure 2.2, the electricity price can be seen for January 1, 2019.

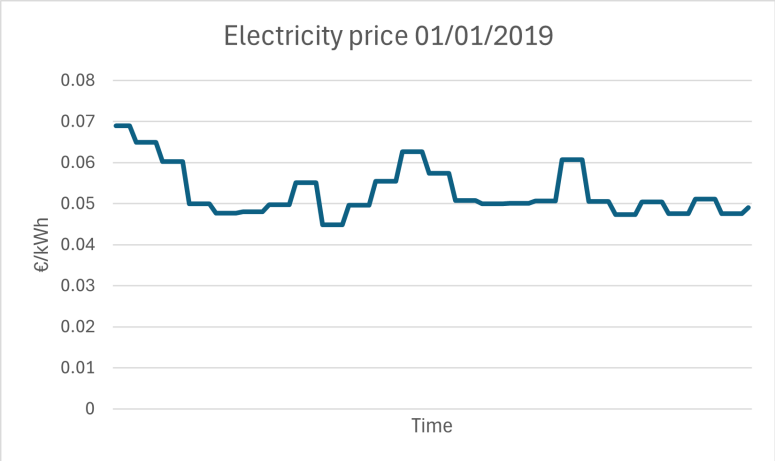

Figure 2.2: Electricity price for January 1st 2019

2.2.4. Flight Schedule

The flight schedule provided by RTHA is a crucial piece to correctly solve the optimization. Many parameters are reliant on the information provided in the flight schedule, such as turnaround time, mission energy needs, flight type categories, unique flight keys, and energy arrival estimates.
The original unedited version of the flight schedule counts 37,542 flights during the duration of 2019.

The goal is to determine which flights could be feasibly replaced by electric aircraft. This research specifically aims to assess whether an existing flight schedule designed for conventional kerosene-powered airplanes can be adapted for electric alternatives. Because electric aircraft generally have lower passenger capacity, a commercial route operated by a Boeing 737 with 180 passengers, for example, might require two electric aircraft flights using the Elysian, which is rated for 90 passengers, to carry the same number of passengers. Therefore, this analysis focuses only on the feasibility of replacement based on flight range and, to a limited extent, passenger capacity, rather than overall passenger throughput.

Original Flight Schedule

Before any calculations and manipulations can be done, the original flight schedule should be cleaned up. Here, multiple columns can be removed for readability and smaller file size. The useful columns present in the original flight schedule are:

- **Flight Number**:
  Specific code an airline assigns to a flight.
- **Aircraft Registration Number**:
  Identifies a specific aircraft.
- **Aircraft Type**:
  Specifies the aircraft model (i.e. B737 = Boeing 737).
- **Airport**:
  Specifies the airport where the aircraft came from or is flying to depending on the traffic type.
- **Traffic Type**:
  Specifies if the flight is arriving, departing, or is a terrain type (i.e. medical helicopters).
- **Scheduled date/time**:
  Specifies the scheduled date/time that the flight arrives/departs.
- **Actual date/time**:
  Specifies the actual date/time that the flight arrives/departs.
- **Status**:
  Specifies whether the aircraft has landed or departed.

One of the columns contains information about the number of passengers on the flight. It is used for filtering the LANDED and DEPARTED pairs that define the turnaround time. In the end, the filtering criteria will be based on range, and to a certain extent on passenger capacity. This is done to make a distinction between commercial aviation aircraft, such as a Boeing 737 designed for more than 120 passengers, and smaller commercial aircraft such as the Embraer 175 designed for up to 86 passengers.

Turnaround Time

Now that the relevant columns are identified, the first large filtering will be done by calculating the turnaround time for each flight. One of the issues is that a certain aircraft is used for multiple flights throughout the year, making it difficult to find the correct and corresponding turnaround time for each flight.
The idea here is to group the flights by registration number, arrival/departure date, and on status, which is either LANDED or DEPARTED. Afterwards, the flights will be grouped by their corresponding LANDED and DEPARTED inputs, making it easy to get the turnaround time.

Using the Pandas package, the program sorts by registration number and arrival/departure date. Next, three new columns are added to the CSV to store information, as the goal is to only use the LANDED portion of the flights. These columns will store the turnaround time, the previous airport, and the next airport. Next, the program will group the CSV by registration number and iterate over the rows in the CSV. If a row contains a cell with LANDED, it will temporarily store a landing time and the airport where it came from under the previous airport column.
Next, it looks for the next row that contains a cell with DEPARTED and calculates the turnaround time by calculating the time difference between the landing time and the time associated with the DEPARTED row. Additionally, the airport is saved once again under the column for the next airport.

Now, the flight schedule has a turnaround time associated with each flight in addition to information about the airports.

Flight Distances

To calculate how much energy the aircraft used on the arrival flight, and how much energy it will need to fulfill its next mission, the flight distances have to be determined based on the previously saved airports.
In Python, two packages are used in addition to Pandas: the *airportsdata* package, which contains the airport codes and locations for a wide range of airports, and the *geopy* package, which can do geographical calculations based on latitude and longitude.
The airport codes used in the flight schedule are the four-letter codes defined by the *International Civil Aviation Organization*, or *ICAO* for short. For example, the ICAO code for Schiphol Airport is EHAM, while the most common notation for people outside of aviation is AMS.

First, the *airportsdata* package is loaded in based on the ICAO codes. Then, the latitude and longitude of RTHA are saved. To calculate the distances, the program runs a function that scans for the airport code in the CSV and saves the longitude and latitude. Then, the coordinates for RTHA and of the previous/next airport are put in the *geopy* function to calculate the distance in km. If an airport code is unknown, the program automatically assigns a distance of 0 km. Later, flights labeled as Flight School or General Aviation that were round-trips to RTHA were assigned a random value between 40 and 100 km to estimate the flight lengths.
In the final step, these distances are then put in their respective columns: previous distance and next distance.

Flight Labels

The flight schedule contains information about *all* flights arriving and departing at RTHA. For this thesis, five flight categories are constructed to manage the type of aircraft used. These categories are:

- **Flight School (FS)**: 2-seater aircraft used by the flight schools.
- **General Aviation (GA)**: 2-4 seater aircraft used by private owners at the airport.
- **Business Aviation (BA)**: 9-11 seater aircraft used for business flights.
- **Commercial Aviation (CA)**: large, narrow-body aircraft used for long-distance flights with 40 or more passengers.

The categories and the electric aircraft used to identify them are found in Table 2.3.

Table 2.3: Aviation Category Definition

Category	Electric Aircraft	Battery Capacity	Passengers	Range (km)
FS	Pipistrel Velis Electro [14]	24.8 kWh	2	50 mins
GA	Cessna 172 [15]	300 kWh	4	250
BA	PC-12 [15]	1.7 MWh	11	450
CA	Maeve 1 [16]	7.5 MWh	44	550
CA2	Elysian [17]	14.2 MWh	90	800

One thing to note is that the aircraft used for the GA and BA categories are based off of the non-electric

variants mentioned using the techniques in [15], where the technical specifications for each aircraft were taken into account to simulate an electric variant. The approach used in this paper was also used to obtain an estimate for the battery sizes for commercial aviation aircraft, as those battery sizes are not concretely specified.
With these categories in mind, the types of aircraft in the flight schedule will be determined together with their passenger capacities. Afterwards, each flight will be labeled based on the criteria from the category list, deeming them replaceable by electric aviation. The exception to this will be the commercial flights, as these aircraft will always have a higher potential capacity than the electrical equivalent.

Aircraft Types

To prevent setting wrong labels only based on distance, the passenger capacities for each aircraft type need to be determined. Using Pandas once more, all unique entries from the *Aircraft Type* column can be extracted. Next, with the use of the Grok AI tool, the list of aircraft names was analyzed [18]. Here, it was asked to return a CSV file that contains the aircraft type entries as listed in the flight schedule together with a column specifying the passenger capacity, and whether the aircraft is an airplane, helicopter, or military airplane.
The latter distinctions were needed to remove any aircraft that were not fit for any category of the research. After the list was made, random checks were done to verify if the passenger counts matched the aircraft type, together with the aircraft's purpose of use. From this, several outliers with uncommon naming by RTHA were picked out and corrected afterwards.

Finally, using Pandas, the *Passenger Capacity*, *next_distance* and *previous_distance* columns, filters were assigned for each category based on the parameters from Table 2.3. This leaves one final step for the flight schedule preparation: the flight's energy calculations.

Flight Energy Expenditure

To finalize the flight schedule for its use in the optimization problem, the energy expenditure of the aircraft must be calculated. Each stage of the flight will be considered to get the best estimate, while accounting for energy reserves in unforeseen cases. Every flight goes through the following stages, and each stage has a different power usage:

- Takeoff
- Climbing
- Cruising
- Descent

The efficiencies, powers, and timings for each flight stage are derived from the work in [15]. For the calculations themselves, it is assumed that the total distance from the previous or next flight will be set as the cruising distance. Although the aircraft covers a certain distance during takeoff or landing, this will not be taken into account.
Using the aforementioned powers, flight stage timings, and reserve specifications, a default energy usage is determined for every aircraft, except for the cruising energy, which depends on the distance flown. By using Equation 2.2, where v is velocity and x is distance, and rearranging for time t, the total cruising time is determined. From this, the energy usage during this phase is determined using Equation 2.1.

$$v = \frac{x}{t} \tag{2.2}$$

Now, both the energies for the previous mission and the next mission can be found by adding all the flight's energies together. Then, two columns are added to the CSV called *Energy Needed* and *Energy at Arrival*. The *Energy Needed* column specifies how much energy the aircraft needs to fulfill its next mission, which is also the amount of energy that needs to be provided during the aircraft's turnaround time at RTHA. It is determined by taking the energy calculation for the next mission, and subtracting the energy that was left in the battery at arrival to RTHA.
The *Energy at Arrival* column gives information about the energy left in the battery at arrival. This will later be used to determine the starting state of charge of the aircraft battery. Instead of assuming that every aircraft left the previous airport with a fully charged battery, a randomized energy level is chosen

between the maximum capacity of the battery, and the energy needed for the mission. Equation 2.3 shows the mathematical equivalence. Here, $E_{\text{mission,prev}}$ represents the total energy the aircraft needed to fulfill its previous mission. $E_{\text{departure,prev}}$ is used to denote the energy level with which the aircraft departed the previous airport. Lastly, $E_{\text{batt,max}}$ represents the maximum battery capacity of the aircraft. Together, they determine a different arrival energy at RTHA.

$$E_{\text{mission,prev}} \leq E_{\text{departure,prev}} \leq E_{\text{batt,max}} \tag{2.3}$$

Final Flight Schedule

With all the preparation and filtering done, a total of 4999 flights are eligible for electrification. A breakdown for each category is found in Table 2.4 and Table 2.5. Here, it can be seen that the highest number of CA2 flights are found during the winter and spring seasons. This could be explained by flights flying, on average, a further distance during the holiday seasons, which with the limited range of Elysian, lowers the CA2 count. In addition, an average for each month considered in the simulations is provided, which was rounded to the nearest integer.

Table 2.4: Flight Count Overview

	Season Data				**Week Average**			
Time Frame	**FSGA**	**BA**	**CA**	**CA2**	**FSGA**	**BA**	**CA**	**CA2**
Year	2788	240	1532	439	54	5	29	8
Winter	467	49	377	241	39	4	31	20
Spring	778	64	461	175	65	5	38	15
Summer	912	63	320	13	76	5	27	1
Fall	630	64	374	10	52	5	31	4

Table 2.5: Detailed Flight Count

	Month Data				**Week Average**			
Time Frame	**FSGA**	**BA**	**CA**	**CA2**	**FSGA**	**BA**	**CA**	**CA2**
January	130	20	135	92	30	5	31	21
April	296	22	151	27	68	5	35	6
July	321	25	101	7	74	6	23	2
October	214	22	141	4	49	5	33	1

3

Methodology

With the prepared data sets, the model can be built. In this chapter, the proposed Mixed-Integer Linear Programming (MILP) model will be discussed. A linear approach was chosen due to the size of the problem. With a linear model, a solution can be found quicker compared to a nonlinear programming (NLP) model. The tradeoff is a faster solution speed with a slight loss in accuracy, as the formulas used in a linear approach cannot be complex. This means that the use of factors with variables, logarithmic functions, geometric functions, and exponential functions is not allowed.
First, the objective of the optimization will be discussed, followed by the constraints used to guide the problem to a viable solution. The variables used in the objective function and its breakdown can be found in Table 3.1.

Table 3.1: Constants, Parameters, and Variables for the objective function.

Symbol	Type	Domain/Value	Units	Description
Constants				
Γ_{deg}	Constant	1/15000	kWh/kWh	BESS degradation rate
$C_{1\text{kWh}}$	Constant	200	€/kWh	Price for 1 kWh of installed BESS
λ_{delay}	Constant	17.78	€/minute	Flight delay penalty
λ_{cancel}	Constant	20930	€/flight	Flight cancellation penalty
Δt	Constant	0.25	h/timestep	Conversion factor from quarter to hour
Parameters				
$\lambda_{\text{grid}}(t)$	Parameter	$\mathbb{R}_{\geq 0}$	€/kWh	Electricity price per kWh
$\lambda_{\text{buy}}(t)$	Parameter	$\lambda_{\text{grid}}(t)$	€/kWh	Electricity buy price per kWh
$\lambda_{\text{sell}}(t)$	Parameter	$0.98 \cdot \lambda_{\text{grid}}(t)$	€/kWh	Electricity sell price per kWh
Variables				
C_{total}	Variable	$\mathbb{R}_{\geq 0}$	€	Total operational cost
C_{grid}	Variable	$\mathbb{R}_{\geq 0}$	€	Total electricity cost from grid
$C_{\text{BESS,deg}}$	Variable	$\mathbb{R}_{\geq 0}$	€	BESS degradation cost
C_{delay}	Variable	$\mathbb{R}_{\geq 0}$	€	Flight delay cost
C_{cancel}	Variable	$\mathbb{R}_{\geq 0}$	€	Flight cancellation cost
$C_{\text{PV,curt}}$	Variable	$\mathbb{R}_{\geq 0}$	€	Curtailed PV cost
$P_{\text{grid}}^{\text{imp}}(t)$	Variable	$\mathbb{R}_{\geq 0}$	kW	Grid import power
$P_{\text{grid}}^{\text{exp}}(t)$	Variable	$\mathbb{R}_{\geq 0}$	kW	Grid export power
$\theta_{\text{BESS}}^{\text{dch}}(t)$	Variable	$\mathbb{R}_{\geq 0}$	kWh	Discharge energy throughput of BESS

Continued on next page

Table 3.1 – Continued from previous page

Symbol	Type	Domain/Value	Units	Description
$P_{\text{BESS}}^{\text{dch}}(t)$	Variable	$\mathbb{R}_{\geq 0}$	kW	BESS discharging power
$T_{\text{delay}}(f)$	Variable	$\mathbb{R}_{\geq 0}$	minutes	Delay in minutes for flight
$\delta_{\text{cancel}}(f)$	Binary	{0,1}	-	1 if flight is canceled
$P_{\text{PV}}^{\text{curt}}(t)$	Variable	$\mathbb{R}_{\geq 0}$	kW	Curtailed PV power

3.1. Objective Function

The model's objective function is to minimize the cost of energy and operations at the airport while calculating an optional BESS sizing. The costs of the objective include the grid energy cost C_{grid}, the BESS degradation cost $C_{\text{BESS.deg}}$, flight delay costs C_{delay}, flight cancellation costs $C_{\text{cancellation}}$, and a PV curtailment cost $C_{\text{PV,curt}}$. In full, the objective function becomes:

$$\min(C_{\text{total}}) = C_{\text{grid}} + C_{\text{BESS,deg}} + C_{\text{delay}} + C_{\text{cancellation}} + C_{\text{PV,curt}} \tag{3.1}$$

In the following sections, each cost in the objective function will be discussed. Here, the factor Δt will be used to denote the timestep, which is 15 minutes. This will correctly translate powers to energy for the associated costs.

1. Grid Energy Cost

One part of the operational costs is the grid electricity cost. Electricity can either be imported from the grid or exported to it. The import and export powers are distinctively used, as the import and export limits are different, as well as the price of the electricity.

$$C_{grid} = \sum_{t}^{T} P_{\text{grid}}^{\text{imp}}(t)\Delta t \lambda_{\text{buy}}(t) - \sum_{t}^{T} P_{\text{grid}}^{\text{exp}}(t)\Delta t \lambda_{\text{sell}}(t) \tag{3.2}$$

2. BESS Degradation Cost

The cost of battery system degradation is calculated to account for the loss of capacity due to usage. This degradation cost is based on the lost capacity at the end of the simulation, which is then multiplied by the cost of acquisition of 1 kWh of BESS, which is between 200-250 €/kWh [19]:

$$C_{\text{BESS,deg}} = Q_{\text{loss}} C_{\text{1kWh}} \tag{3.3}$$

Here, Q_{loss} denotes the lost capacity of the BESS. It is calculated based on the warranty specifications for the Tesla Powerpack [20]. Here, it is noted that the battery pack will be at 70% of its original capacity after 4469 cycles, which is rounded to 4500 cycles for this study. With these parameters, a factor can be calculated to denote the amount of capacity lost in kWh, per kWh cycled through the battery by discharging. This is done by dividing the capacity loss of 30% by the number of cycles needed for this loss, as seen in Equation 3.4. With this, a capacity loss factor of $\frac{1}{15000}$ is found.

$$\Gamma_{\text{deg}} = \frac{30\% \text{ capacity loss}}{4500 \text{ cycles}} = \frac{1}{15000} \frac{\text{kWh lost}}{\text{kWh cycled}} \tag{3.4}$$

Lastly, this capacity loss factor is multiplied by the total amount of energy discharged from the BESS during the simulation to find the actual capacity loss of the system.

$$Q_{\text{loss}} = \Gamma_{\text{deg}} \theta_{\text{BESS}}^{\text{dch}} \tag{3.5}$$

$$\theta_{\text{BESS}}^{\text{dch}}(t) = P_{\text{BESS}}^{\text{dch}}(t)\Delta t \tag{3.6}$$

3. Delay Cost

One of the most important costs for the optimization is the delay cost. They are needed for the planner as delays could be expected with electric aviation. This is due to maximum charging C-rates, short turnaround times, and power balances. With this, the program will penalize the objective when a flight

has to be delayed beyond its original turnaround time. On the EUROCONTROL website, prices for flight delays can be found [21]. Here, there are two types of delay costs: strategic delays, costing 17.78 €/minute, are planned and accounted for in scheduling to minimize overall impact, while tactical delays, at 166 €/minute, are unexpected delays that occur on the day of operation and include immediate costs like passenger compensation and operational disruptions.
Because the goal of the research is to plan the implementation of electric aviation, the lower delay price due to strategic delay planning will be used, where delays can help with charging or aircraft.

To determine a given flight's delay, the optimizer can calculate the extra time needed past its turnaround time. Then, this extra time is converted to minutes, a summation is made over all flights and multiplied by the delay penalty. The model also imposes a strict maximum extension period of 3 hours. This is done to reduce the delay times and also to increase the solving speed, as there are fewer solutions to assess.

$$C_{\text{delay}} = \sum_{f}^{F} T_{\text{delay}}(f)\lambda_{\text{delay}} \tag{3.7}$$

4. Cancellation Cost

Whenever a flight cannot be charged within its turnaround time and the possible 3-hour extension, it is automatically canceled. In another chapter on the EUROCONTROL website, prices of flight cancellations are found [22]. To remove the need for definitions of aircraft, the average cancellation cost of € 20,930 per flight was taken. When a flight gets canceled, the model automatically sets its energy needs to 0 kWh to prevent the aircraft from charging and taking energy from the system. Another variable is then triggered to count the number of canceled flights. In the objective function, this cancellation cost is multiplied by the number of canceled flights to obtain the total price.

$$C_{\text{cancellation}} = \sum_{f}^{F} \delta_{\text{cancel}}(f)\lambda_{\text{cancellation}} \tag{3.8}$$

5. Curtailment Cost

The final cost is the one for the curtailment of power from the PV system. Although the curtailment of PV systems is not as straightforward as that of wind turbines, it is still considered to add incentive for the solver to maximize power use from the PV park. Here, it is assumed that parts of the PV park can be disconnected, lowering the total power output. This is included to incentivize the model to use as much PV power as possible, but also to account for the rare occasions where there is an abundance of PV power, where not all of it can be used in the system. In those cases, the model pays the market price for each kWh of PV energy not utilized. This cost can be found in Equation 3.9.

$$C_{\text{PV,curt}} = P_{\text{PV,curt}}(t)\lambda_{\text{buy}}(t)\Delta t \tag{3.9}$$

3.1.1. Weighted Costs

As a final step, weights were added to the model to prioritize the lowering of certain costs. The weights can be found in Table 3.2. The highest weight is linked to the cancellation cost, as the goal is to achieve a flight schedule with electric flights that matches the original as closely as possible. Secondly, a lower weight is given to the delay costs for the same reason as the cancellation cost. Lastly, the weights for grid cost, BESS degradation, and PV curtailment stay at 1, as they have no higher priority.

For the final results the prices are stated in their original form, where they were divided by their respective weights after the optimization has concluded. With these weights, the final objective function can be expressed as:

$$\min(C_{\text{total}}) = \omega_{\text{grid}}C_{\text{grid}} + \omega_{\text{BESS,deg}}C_{\text{BESS}} + \omega_{\text{delay}}C_{\text{delay}} + \omega_{\text{cancel}}C_{\text{cancel}} + \omega_{\text{PV,curt}}C_{\text{PV,curt}} \tag{3.10}$$

Table 3.2: Objective function cost weights.

Cost Type	Expression	Weight
Grid Cost	ω_{grid}	1
BESS Degradation	$\omega_{\text{BESS,deg}}$	1
Curtailment	$\omega_{\text{PV,curt}}$	1
Delay	ω_{delay}	3
Cancellation	ω_{cancel}	10

3.2. Constraints

The optimization model for the airport's energy infrastructure requires constraints to ensure feasible and practical solutions while staying within the limitations of operation. By adding these boundaries, the model can generate flight strategies while minimizing the cost of operations. This section will give a detailed outline of the constraints used in the optimization problem in their respective categories.
In Table 3.3, a complete overview of the constants, parameters, and variables is found with their descriptions for the optimization.

Table 3.3: Constants, Parameters, and Variables for the Optimization Model

Symbol	Type	Domain/Value	Units	Description
Preprocessed Parameters				
$P_{\text{PV}}(t)$	Parameter	$\mathbb{R}_{\geq 0}$	kW	PV power at time t
$P_{\text{airport}}(t)$	Parameter	$\mathbb{R}_{\geq 0}$	kW	Airport demand at time t
$\lambda_{\text{market}}(t)$	Parameter	$\mathbb{R}_{\geq 0}$	€/kWh	Electricity market price at time t
Global Constants				
Δt	Constant	0.25	h/timestep	Conversion factor from quarter to hour
Δt_{h2m}	Constant	60	minutes/h	Conversion factor from hours to minutes
ω_{grid}	Constant	1	-	Weight for grid cost
$\omega_{\text{BESS,deg}}$	Constant	1	-	Weight for degradation
$\omega_{\text{PV,curt}}$	Constant	1	-	Weight for curtailment cost
ω_{delay}	Constant	3	-	Weight for delay cost
ω_{cancel}	Constant	10	-	Weight for cancellation cost
$T_{\text{start}}^{\text{sim}}$	Constant	Differs per simulation	Date	Starting time of simulation
$T_{\text{end}}^{\text{sim}}$	Constant	Differs per simulation	Date	Ending time of simulation
PV Variables				
$P_{\text{PV}}^{\text{curt}}(t)$	Variable	$\mathbb{R}_{\geq 0}$	kW	Curtailed PV power
Grid Constants				
$P_{\text{grid}}^{\text{max,imp}}$	Constant	3500	kW	Grid import limit
$P_{\text{grid}}^{\text{max,exp}}$	Constant	7500	kW	Grid export limit
Grid Variables				
$P_{\text{grid}}^{\text{imp}}(t)$	Variable	$\mathbb{R}_{\geq 0}$	kW	Grid import power
$P_{\text{grid}}^{\text{exp}}(t)$	Variable	$\mathbb{R}_{\geq 0}$	kW	Grid export power
$\delta_{\text{grid}}^{\text{imp}}(t)$	Binary	{0,1}	-	Grid import/export exclusivity
BESS Constants				

Continued on next page

Table 3.3 – Continued from previous page

Symbol	Type	Domain/Value	Units	Description
$C_{1\text{kWh}}$	Constant	200	€/kWh	Price for 1 kWh of installed BESS
Γ_{deg}	Constant	1/15000	kWh/kWh	Degradation rate of BESS
$R^{\text{ch}}_{\text{BESS}}$	Constant	2	-	Maximum charging C-rate for BESS
$R^{\text{dch}}_{\text{BESS}}$	Constant	2	-	Maximum discharging C-rate for BESS
BESS Variables				
Q_{BESS}	Variable	[500, 20000]	kWh	BESS capacity size
$Q^{\text{eff}}_{\text{BESS}}(t)$	Variable	$\mathbb{R}_{\geq 0}$	kWh	Effective BESS capacity
$E_{\text{BESS}}(t)$	Variable	$\mathbb{R}_{\geq 0}$	kWh	Energy level of BESS
$P^{\text{ch}}_{\text{BESS}}(t)$	Variable	$\mathbb{R}_{\geq 0}$	kW	BESS charging power
$P^{\text{dch}}_{\text{BESS}}(t)$	Variable	$\mathbb{R}_{\geq 0}$	kW	BESS discharging power
$\delta^{\text{dch}}_{\text{BESS}}(t)$	Binary	{0,1}	kW	BESS charge/discharge exclusivity
Q_{loss}	Variable	$\mathbb{R}_{\geq 0}$	kWh	Capacity loss of BESS
$\theta^{\text{dch}}_{\text{BESS}}(t)$	Variable	$\mathbb{R}_{\geq 0}$	kWh	Discharge energy throughput of BESS
Flight Schedule Constants				
λ_{delay}	Constant	17.78	€/minute	Flight delay penalty
λ_{cancel}	Constant	20930	€/flight	Flight cancellation penalty
Flight Schedule Parameters				
$T^{\text{og}}_{\text{turn}}(f)$	Parameter	$\mathbb{R}_{\geq 0}$	h	Original turnaround time in flight schedule
$T_{\text{arr}}(f)$	Parameter	$\mathbb{R}_{\geq 0}$	h	Arrival time in flight schedule
Flight Schedule Variables				
$T_{\text{turn}}(f)$	Variable	$[T^{\text{og}}_{\text{turn}}, T^{\text{og}}_{\text{turn}}+1] \in$ FS,GA,BA $[T^{\text{og}}_{\text{turn}}, T^{\text{og}}_{\text{turn}}+3] \in$ CA,CA2	h	Actual turnaround time
$T_{\text{delay}}(f)$	Variable	$\mathbb{R}_{\geq 0}$	minutes	Delay in minutes for flight
$\delta^{\text{start}}_{\text{ch}}[f,t]$	Binary	{0,1}	-	1 if flight starts charging at time t
$\delta_{\text{ch}}[f,t]$	Binary	{0,1}	-	1 if flight is charging at time t
$\delta_{\text{cancel}}(f)$	Binary	{0,1}	-	1 if flight is canceled
$\delta_{\text{can\_charge}}(f)$	Binary	{0,1}	-	1 if flight is eligible for charging
$T^{\text{ch}}_{\text{start}}(f)$	Variable	$\mathbb{R}_{\geq 0}$	-	Timestep where flight starts charging
$T^{\text{ch}}_{\text{end}}(f)$	Variable	$\mathbb{R}_{\geq 0}$	-	Timestep where flight stops charging
$D_{ch}(f)$	Variable	$\mathbb{R}_{\geq 0}$	-	Number of charging timestep intervals
Charge Profile Constants				
$R^{\text{ch,max}}_{\text{aircraft}}$	Constant	1.5	-	Maximum charging C-rate for aircraft

Continued on next page

Table 3.3 – Continued from previous page

Symbol	Type	Domain/Value	Units	Description
Charge Profile Parameters				
$B_{\text{cap}}(f)$	Parameter	$\mathbb{R}_{\geq 0}$	kWh	Battery capacity of aircraft
$P^{\text{ch}}_{\text{max}}(f)$	Parameter	$R^{\text{ch,max}}_{\text{aircraft}}(f)B_{\text{cap}}(f)$	kW	Maximum charge power for aircraft
$SoC_{\text{init}}(f)$	Parameter	[0, 100]	%	Initial SoC of aircraft at arrival
$SoC_{\text{tran}}(f)$	Parameter	80	%	Transition SoC for CPCV charging
$E_{\text{needed}}(f)$	Parameter	$\mathbb{R}_{\geq 0}$	kWh	Energy needed to charge aircraft
Charge Profile Variables				
$R^{\text{ch}}_{\text{aircraft}}(f)$	Variable	[0, 1.5]	-	Charging C-rate for aircraft
$SoC[f,t]$	Variable	[0, 100]	%	SoC of aircraft at time t
$E_{\text{delivered}}[f,t]$	Variable	$\mathbb{R}_{\geq 0}$	kWh	Energy delivered to aircraft over time t
$E_{\text{slack}}(f)$	Variable	$\mathbb{R}_{\geq 0}$	kWh	Energy not provided to aircraft
$P^{\text{ch}}_{\text{CP}}[f,t]$	Variable	$\mathbb{R}_{\geq 0}$	kW	Charge power during CP phase
$P^{\text{ch}}_{\text{CV}}[f,t]$	Variable	$\mathbb{R}_{\geq 0}$	kW	Charge power during CV phase
$P^{\text{ch}}_{\text{CPCV}}[f,t]$	Variable	$\mathbb{R}_{\geq 0}$	kW	Charge power during CPCV
$P^{\text{ch,tot}}_{\text{flights}}(t)$	Variable	$\mathbb{R}_{\geq 0}$	kW	Total charge power of flights at time t
$\delta_{\text{CV}}[f,t]$	Binary	{0,1}	-	1 if aircraft is in CV phase
Sets				
F	Set	Set of flights	Unitless	All flights within simulation
F_{active}	Set	Subset of F	Unitless	Flights that can be charged during simulation
T	Set	Set of timesteps	Unitless	Stores the timesteps of the simulation

Constraint Equations

The following section will define the constraints for the energy management optimization model, based on the parameters, variables, and sets provided. Constraints are grouped by component and reflect the relationships between the parameters and variables found in the overview table. In the constraint overview, the constraints are written in their normal mathematical form for easy readability. Then, a section explaining the linearization of the nonlinear constraints can be found. To conclude, a subsection explaining the pre-processing of variables to reduce memory usage can be found.

1. Power Balance Constraints

The power balance ensures that supply (PV, grid import, BESS discharging) meets demand (load, grid export, BESS charging, flight charging) at each time step t.

$$P^{\text{imp}}_{\text{grid}}(t) + P^{\text{dch}}_{\text{BESS}}(t) + P_{\text{PV}}(t) - P^{\text{curt}}_{\text{PV}}(t) = P^{\text{exp}}_{\text{grid}}(t) + P^{\text{ch}}_{\text{BESS}}(t) + P_{\text{airport}}(t) + P^{\text{ch,tot}}_{\text{flights}}(t) \quad \forall t \tag{3.11}$$

where $P^{\text{ch,tot}}_{\text{flights}}(t) = \sum_{f \in F_{active}} P^{\text{ch}}_{\text{CPCV}}[f,t]$ represents the total charging power for active flights.

2. PV Constraints

PV curtailment is limited by available PV generation. If there is an excess amount of PV power, the curtailment variable gets a value. Equation 3.12 ensures that the curtailed power will not exceed the generated PV power at any timestep.

$$0 \leq P_{\mathrm{PV}}^{\mathrm{curt}}(t) \leq P_{\mathrm{PV}}(t) \quad \forall t \tag{3.12}$$

3. Grid Constraints

Grid import and export are restricted by maximum limits, and exclusivity ensures that import and export do not occur simultaneously. The RTHA grid connection is rated for 10 MVA. However, from correspondence and meetings it became clear that only around 3.5 MVA is available for import. For export, a value of 7.5 MVA is chosen to slightly account for grid congestion and limit the amount of export power.

Equation 3.13 and Equation 3.14 ensure that the imported and exported power do not exceed the limits imposed on them by $P_{\mathrm{grid}}^{\mathrm{max,imp}}$ and $P_{\mathrm{grid}}^{\mathrm{max,exp}}$, while $\delta_{\mathrm{grid}}^{\mathrm{imp}}(t)$ maintains exclusivity. This exclusivity prevents the system from importing and exporting power to the grid at the same time.

$$0 \leq P_{\mathrm{grid}}^{\mathrm{imp}}(t) \leq P_{\mathrm{grid}}^{\mathrm{max,imp}} \cdot \delta_{\mathrm{grid}}^{\mathrm{imp}}(t) \quad \forall t \tag{3.13}$$

$$0 \leq P_{\mathrm{grid}}^{\mathrm{exp}}(t) \leq P_{\mathrm{grid}}^{\mathrm{max,exp}} \cdot (1 - \delta_{\mathrm{grid}}^{\mathrm{imp}}(t)) \quad \forall t \tag{3.14}$$

4. Battery Energy Storage (BESS) Constraints

The BESS constraints are set up to model energy evolution, charge / discharge limits, capacity limits, and degradation during simulation.
In Equation 3.15, the effective capacity of the BESS is modeled. First, the capacity is set to the optimized version; afterwards, the degradation caused by discharging the battery is taken into account by the factor $Q_{\mathrm{loss}}(t)$. Equation 3.16 and Equation 3.17 break down the functionality of this factor.

$$Q_{\mathrm{BESS}}^{\mathrm{eff}}(t) = \begin{cases} Q_{\mathrm{BESS}}, & \text{for t = } T_{\mathrm{start}}^{\mathrm{sim}} \\ Q_{\mathrm{BESS}}^{\mathrm{eff}}(t-1) - Q_{\mathrm{loss}}(t), & \text{for t > } T_{\mathrm{start}}^{\mathrm{sim}} \end{cases} \tag{3.15}$$

$$\theta_{\mathrm{BESS}}^{\mathrm{dch}}(t) = P_{\mathrm{BESS}}^{\mathrm{dch}}(t)\Delta t \quad \forall t \tag{3.16}$$

$$Q_{\mathrm{loss}}(t) = \Gamma_{\mathrm{deg}}\theta_{\mathrm{BESS}}^{\mathrm{dch}}(t) \quad \forall t \tag{3.17}$$

In Equation 3.18 and Equation 3.19 the charging and discharging powers of the battery are limited by their imposed C-rates $R_{\mathrm{BESS}}^{\mathrm{ch}}$ and $R_{\mathrm{BESS}}^{\mathrm{dch}}$, while $\delta_{\mathrm{BESS}}^{\mathrm{ch}}$ ensures exclusivity between charging and discharging of the battery.

$$0 \leq P_{\mathrm{BESS}}^{\mathrm{ch}}(t) \leq R_{\mathrm{BESS}}^{\mathrm{ch}} Q_{\mathrm{BESS}}^{\mathrm{eff}}(t) \delta_{\mathrm{BESS}}^{\mathrm{ch}}(t) \quad \forall t \tag{3.18}$$

$$0 \leq P_{\mathrm{BESS}}^{\mathrm{dch}}(t) \leq R_{\mathrm{BESS}}^{\mathrm{dch}} Q_{\mathrm{BESS}}^{\mathrm{eff}}(t)(1 - \delta_{\mathrm{BESS}}^{\mathrm{ch}}(t)) \quad \forall t \tag{3.19}$$

To ensure that the BESS has a safe Depth-of-Discharge (DoD), upper and lower bounds are set on the SoC of the battery, which range from 10%-100%, as seen in Equation 3.20. Equation 3.21 models the energy evolution of the BESS. The previous energy state is used in combination with the power charged or discharged to calculate the new energy level. Here, Δt is applied to correctly convert the timestep powers to kWh values.

$$0.1 \cdot Q_{\mathrm{BESS}}^{\mathrm{eff}}(t) \leq E_{\mathrm{BESS}}(t) \leq Q_{\mathrm{BESS}}^{\mathrm{eff}}(t) \quad \forall t \tag{3.20}$$

$$E_{\mathrm{BESS}}(t) = E_{\mathrm{BESS}}(t-1) + \Delta t \cdot (P^{\mathrm{ch}}_{\mathrm{BESS}}(t-1) - P^{\mathrm{dch}}_{\mathrm{BESS}}(t-1)) \quad \forall t \tag{3.21}$$

Lastly, Equation 3.22 sets the starting energy level of the BESS, which corresponds to 50%. Because the BESS sizing is not considered as operational cost, it is not taken into account in the objective function. This results in the program always choosing the upper bound of 20 MWh capacity. A two-step approach is utilized for the BESS size and will be discussed in section 4.1. However, to prevent biases from the starting energy point, an equal ending energy level of 50% must be reached. This also ensures that the starting point of the BESS is not regarded as 'free' energy given by the optimizer definition, but as a viable option in real-life operations.

$$E_{\mathrm{BESS}}(t) = \begin{cases} 0.5 \cdot Q^{\mathrm{eff}}_{\mathrm{BESS}}(t), & \text{for t = } T^{\mathrm{sim}}_{\mathrm{start}} \\ 0.5 \cdot Q^{\mathrm{eff}}_{\mathrm{BESS}}(t), & \text{for t = } T^{\mathrm{sim}}_{\mathrm{end}} \end{cases} \tag{3.22}$$

5. Flight Scheduling Constraints

Flight scheduling constraints manage the scheduling of flights, charging power of aircraft, state of charge, charging phases, delays, and cancellation.

Equation 3.23 states that the optimized turnaround time must be greater or equal to the original turnaround time. It is not possible for a flight to have a shorter turnaround time, as that will also impact the workings of the flight schedule and charging power peaks due to shorter turnaround times. Equation 3.24 ensures that, when charging occurs, it happens between arrival and departure. It is important to note that the departure time is set with $T_{\mathrm{turn}}(f)$, as its optimized value is later used in delay calculations if it has exceeded $T^{\mathrm{og}}_{\mathrm{turn}}$.

$$T_{\mathrm{turn}}(f) \geq T^{\mathrm{og}}_{\mathrm{turn}}(f) \quad \forall f \in F_{active} \tag{3.23}$$

$$T_{\mathrm{arr}}(f) \leq T^{\mathrm{ch}}_{\mathrm{start}}(f) \leq T_{\mathrm{arr}}(f) + T_{\mathrm{turn}}(f) \quad \forall f \in F_{active} \tag{3.24}$$

Next, Equation 3.25 is used to allow for only exactly one charging starting point, while Equation 3.26 keeps the charging binary variable set to zero if charging has not started yet.

$$\sum_{t} \delta^{\mathrm{start}}_{\mathrm{ch}}[f,t] \leq 1 \quad \forall f \in F_{active} \tag{3.25}$$

$$\delta_{\mathrm{ch}}[f,t] \leq \sum_{\tau = T_{\mathrm{arr}}(f)} \delta^{\mathrm{start}}_{\mathrm{ch}}[f,t] \quad \forall f \in F_{active}, \forall t \in D_{ch}(f) \tag{3.26}$$

Equation 3.27 then sets the timestep at the start of charging, based on $\delta^{\mathrm{start}}_{\mathrm{ch}}[f,t]$. If the optimized turnaround time exceeds the original one, Equation 3.28 is used to calculate the delay in minutes for that flight. Lastly, Equation 3.29 ensures that the binary variable for charging stays at 1 from the start of charging until departure. When a flight cannot charge in one simultaneous period, this constraint allows for the continuation of charging.

$$T^{\mathrm{ch}}_{\mathrm{start}}(f) = \sum_{t} t \cdot \delta^{\mathrm{start}}_{\mathrm{ch}}[f,t] \quad \forall f \in F_{active} \tag{3.27}$$

$$T_{\mathrm{delay}}(f) = (T_{\mathrm{turn}}(f) - T^{\mathrm{og}}_{\mathrm{turn}}(f))\Delta t_{\mathrm{h2m}} \quad \forall f \in F_{active} \tag{3.28}$$

$$\delta_{\mathrm{ch}}[f,t] = \begin{cases} 1, & T^{\mathrm{ch}}_{\mathrm{start}}(f) \leq t \leq T_{\mathrm{arr}}(f) + T_{\mathrm{turn}}(f) \\ 0, & \text{otherwise} \end{cases} \tag{3.29}$$

The charge power at any time during the charging duration is summarized in Equation 3.30, where it is the sum of the CP power and CV power.

$$P^{\text{ch}}_{\text{CPCV}}[f,t] = P^{\text{ch}}_{\text{CP}}[f,t] + P^{\text{ch}}_{\text{CV}}[f,t] \quad \forall f \in F_{active}, \forall t \in D_{ch}(f) \tag{3.30}$$

Equations (3.31) and (3.32) restrict the charging power during each phase to a maximum limit based on $B_{\text{cap}(f)}$ and $R^{\text{ch,max}}_{\text{aircraft}}$.

$$P^{\text{ch}}_{\text{CP}}[f,t] \leq P^{\text{ch}}_{\text{max}}(f) \quad \forall f \in F_{active}, \forall t \in D_{ch}(f) \tag{3.31}$$

$$P^{\text{ch}}_{\text{CV}}[f,t] \leq P^{\text{ch}}_{\text{max}}(f) \quad \forall f \in F_{active}, \forall t \in D_{ch}(f) \tag{3.32}$$

To protect the aircraft batteries from unnecessary stress, a Constant Power - Constant Voltage (CPCV) charging profile is used. In this profile, the battery is charged at a constant power until a certain transition SoC, $SoC_{\text{tran}}(f)$, is reached. Here, that value is set to 80%. When this threshold has been reached, the charging profile switches into the Constant Voltage stage, where it gradually lowers the charging current at the end of charging when the terminal voltages of the battery cells are at its maximum value until the battery is sufficiently charged. A study has shown that CPCV has a slightly higher usable energy efficiency compared to the widely used Constant Current - Constant Voltage (CCCV) charging profile [23]. Figure 3.1 shows an example of the CPCV charging profile.

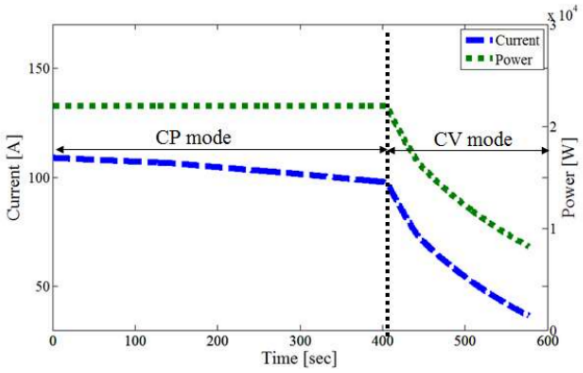

Figure 3.1: Example of a CPCV charging curve. [23]

The logic behind the CPCV charging profile is found in Equations (3.33) and (3.34). For the CP phase, the optimizer chooses a C-rate $R^{\text{ch}}_{\text{aircraft}}(f)$. In the CV phase, the same CP power is applied together with a drop-off factor based on $SoC[f,t]$. Here, SoC_{max} denotes the maximum SoC an aircraft can reach, which is always 100%. Lastly, $\delta_{\text{CV}}[f,t])$ is utilized to correctly switch from CP phase to CV phase based on the logic in Equation 3.35. The constraints that define the CPCV charging profile are nonlinear due to the multiplication of the variables $R^{\text{ch}}_{\text{aircraft}}(f)$ and $SoC[f,t]$.

$$P^{\text{ch}}_{\text{CP}}[f,t] = R^{\text{ch}}_{\text{aircraft}}(f) B_{\text{cap}}(f) \cdot (1 - \delta_{\text{CV}}[f,t]) \quad \forall f \in F_{active}, \forall t \in D_{ch}(f) \tag{3.33}$$

$$P^{\text{ch}}_{\text{CV}}[f,t] = \frac{R^{\text{ch}}_{\text{aircraft}}(f) B_{\text{cap}}(f)}{1 - SoC_{\text{tran}}(f)} \cdot (1 - \frac{SoC[f,t]}{SoC_{\text{max}}}) \cdot \delta_{\text{CV}}[f,t] \quad \forall f \in F_{active}, \forall t \in D_{ch}(f) \tag{3.34}$$

$$\delta_{\text{CV}}[f,t] = \begin{cases} 1 & \text{if } SoC[f,t] > SoC_{\text{tran}}(f) \\ 0 & \text{otherwise} \end{cases} \quad \forall f \in F_{active}, \forall t \in D_{ch}(f) \tag{3.35}$$

Lastly, to handle the cancellation of flights, the delivered energy to each aircraft must be monitored. With the energy level, the state of charge can be determined, which in turn acts as a variable in the

CPCV charging profile.
In Equation 3.36, the delivered energy to an aircraft is calculated based on the charging power used. With $E_{\text{delivered}}[f,t]$ in place, the SoC evolution is determined by Equation 3.37.

$$E_{\text{delivered}}[f,t] = \begin{cases} 0, & \text{for t = } T^{\text{ch}}_{\text{start}}(f) \\ E_{\text{delivered}}[f,t-1] + P^{\text{ch}}_{\text{CPCV}}[f,t]\Delta t, & \text{for t > } T^{\text{ch}}_{\text{start}}(f) \end{cases} \tag{3.36}$$

$$SoC[f,t] = \begin{cases} SoC_{\text{init}}(f), & \text{for t = } T^{\text{ch}}_{\text{start}}(f) \\ SoC_{\text{init}}(f) + \frac{E_{\text{delivered}}[f,t]}{B_{\text{cap}}(f)}, & \text{for t > } T^{\text{ch}}_{\text{start}}(f) \end{cases} \quad \forall f \in F_{active}, \forall t \in D_{ch}(f) \tag{3.37}$$

Equation 3.38 looks at the energy level after the final charging step. If the energy required for a mission is not met after the theoretical turnaround time, the $E_{\text{slack}}(f)$ variable will have a nonzero value. As a result of this, the flight lacks sufficient energy for its upcoming mission and should therefore be canceled. Equation 3.39 shows that the binary variable for flight cancellation $\delta_{\text{cancel}}(f)$ will be set to 1 when the required energy is not provided. This in turn sets the variable $E_{\text{delivered}}[f,t]$ for this flight to zero, together with the charging power seen in Equation 3.40. Now, the model will not take the canceled flight into account in the charging schedule and flag it as canceled.

$$E_{\text{delivered}}[f, T^{\text{ch}}_{\text{end}}(f)] + E_{\text{slack}}(f) \geq E_{\text{needed}}(f) \cdot (1 - \delta_{\text{cancel}}(f)) \quad \forall f \in F_{active} \tag{3.38}$$

$$\delta_{\text{cancel}}(f) = \begin{cases} 1 & \text{if } E_{\text{slack}}(f) > 0 \\ 0 & \text{if } E_{\text{slack}}(f) = 0 \end{cases} \quad \forall f \in F_{active} \tag{3.39}$$

$$P^{\text{ch}}_{\text{CPCV}}[f,t] \leq P^{\text{ch}}_{\text{max}}(f) \cdot (1 - \delta_{\text{cancel}}(f)) \quad \forall f \in F_{active}, \forall t \in D_{ch}(f) \tag{3.40}$$

3.3. Linearization of Constraints

To conclude the constraints chapter, the remaining nonlinear constraints have to be made linear to fit the model. To achieve linearity, two methods are used together, namely:

- Big-M Values
- Auxiliary Variables

A Big-M value is used to act as a switch to activate or deactivate constraints in a way like binary variables would. They effectively take a value in a range that the original variable would. It is important to ensure that this value is large enough to not overly restrict the variables while being small enough to avoid numerical problems and overshoot. An example is shown in Equation 3.41.

$$y \leq M \cdot z \tag{3.41}$$

If z is a binary variable, the Big-M value ensures that y can take values up to M when $z = 1$, while still enforcing that $y = 0$ when $z = 0$.

Auxiliary variables are additional variables that translate a nonlinear product of variables into linear ones. These are constrained using multiple linear equations that utilize Big-M values to mimic the logic of the nonlinear relationships.

1. BESS Constraints

This includes Equations (3.18) and (3.19), as they rely on the multiplication of two variables, namely $Q^{\text{eff}}_{\text{BESS}}$ and $\delta^{\text{ch}}_{\text{BESS}}$. Unlike the power grid constraints, the power limits of the BESS are dependent on the capacity, which first needs to be determined by the optimizer.
Table 3.4 lists the auxiliary variables and Big-M values used for the extra BESS constraints.

Table 3.4: Auxiliary variables and Big-M values for BESS linearization.

Symbol	Type	Domain/Value	Units	Description
$P^{\text{lim}}_{\text{BESS,ch}}(t)$	Auxiliary	$\mathbb{R}_{\geq 0}$	kW	Sets upper bound for charging power of BESS
$P^{\text{lim}}_{\text{BESS,dch}}(t)$	Auxiliary	$\mathbb{R}_{\geq 0}$	kW	Sets upper bound for discharging power of BESS
$Q^{\text{dch}}_{\text{BESS}}(t)$	Auxiliary	$\mathbb{R}_{\geq 0}$	kWh	Portion of BESS capacity allocated for discharging
M_{BESS}	Big-M	40000	kW	Maximum power draw of BESS

Equations (3.42) and (3.43) ensure that the charging and discharging powers do not exceed the linearized limits.

$$P^{\text{ch}}_{\text{BESS}}(t) \leq P^{\text{lim}}_{\text{BESS,ch}}(t) \quad \forall t \tag{3.42}$$

$$P^{\text{dch}}_{\text{BESS}}(t) \leq P^{\text{lim}}_{\text{BESS,dch}}(t) \quad \forall t \tag{3.43}$$

Equation 3.44 limits the discharging capacity to the effective battery capacity.

$$Q^{\text{dch}}_{\text{BESS}}(t) \leq Q^{\text{eff}}_{\text{BESS}}(t) \quad \forall t \tag{3.44}$$

Equations (3.45) and (3.46) are the upper and lower bounds ensuring that that the discharging capacity is zero when not discharging, while setting it equal to the effective BESS capacity when it is discharging.

$$Q^{\text{dch}}_{\text{BESS}}(t) \leq M_{\text{BESS}} \cdot \delta^{\text{dch}}_{\text{BESS}}(t) \quad \forall t \tag{3.45}$$

$$Q^{\text{dch}}_{\text{BESS}}(t) \geq Q^{\text{eff}}_{\text{BESS}}(t) - M_{\text{BESS}} \cdot (1 - \delta^{\text{dch}}_{\text{BESS}}(t)) \quad \forall t \tag{3.46}$$

Equation 3.48 defines the discharge power limit based on the discharging capacity and the discharge C-rate. Lastly, Equation 3.48 defines the charge power limit based on the remaining capacity and charge C-rate. Now, the working of the BESS system is fully linear and is ready to be used in the optimization.

$$P^{\text{lim}}_{\text{BESS,dch}}(t) = R^{\text{dch}}_{\text{BESS}} Q^{\text{dch}}_{\text{BESS}}(t) \quad \forall t \tag{3.47}$$

$$P^{\text{lim}}_{\text{BESS,ch}}(t) = R^{\text{ch}}_{\text{BESS}}(Q^{\text{eff}}_{\text{BESS}}(t) - Q^{\text{dch}}_{\text{BESS}}(t)) \quad \forall t \tag{3.48}$$

2. Charging Profile Constraints

The charging profile constraints that are nonlinear are Equations (3.33) and (3.34). Here, there is multiplication of the variables $R^{\text{ch}}_{\text{aircraft}}(f)$, $\delta_{\text{CV}}[f,t]$, and $SoC[f,t]$. In this case, there is added complexity to ensure that the transition between the CP and CV phase stands together with there now being three variables in multiplication with each other.
Table 3.5 lists the auxiliary variables and Big-M values used for the extra CPCV charging constraints.

Table 3.5: Auxiliary variables and Big-M values for CPCV linearization.

Symbol	Type	Domain/Value	Units	Description
$\delta_{\mathrm{CV}}^{\mathrm{ch}}[f,t]$	Binary	{0,1}	-	1 if aircraft is charging in CV phase
$\delta_{\mathrm{CP}}^{\mathrm{ch}}[f,t]$	Binary	{0,1}	-	1 if aircraft is charging in CP phase
$P_{\mathrm{CP}}^{\mathrm{aux}}[f,t]$	Auxiliary	$\mathbb{R}_{\geq 0}$	kW	Auxiliary CP power
$X_{\mathrm{C-rate}}^{\mathrm{dropoff}}[f,t]$	Auxiliary	[0, 7.5]	-	Auxiliary variable for C-rate times drop-off
$P_{\mathrm{CV}}^{\mathrm{base}}[f,t]$	Auxiliary	[0, 7.5]	-	Auxiliary variable for $X_{\mathrm{C-rate}}^{\mathrm{dropoff}}[f,t] \cdot \delta_{\mathrm{CV}}^{\mathrm{ch}}[f,t]$
$X_{\mathrm{dropoff}}[f,t]$	Expression	Equation 3.50	-	Drop-off factor in CV phase
$M_{\mathrm{C-rate}}$	Big-M	1.5	-	Maximum value for charging C-rate
M_{dropoff}	Big-M	5	-	Maximum value for drop-off factor

Before moving on to the constraints, a brief explanation will be provided for the value of M_{dropoff}, which defines the domains for $X_{\mathrm{C-rate}}^{\mathrm{dropoff}}[f,t]$ and $P_{\mathrm{CV}}^{\mathrm{base}}[f,t]$ together with $M_{\mathrm{C-rate}}$.
In Equation 3.34, the power drop-off function of the CV function is given. The drop-off part is given in Equation 3.49. Here, $SoC_{\mathrm{tran}}(f)$ and $SoC_{\mathrm{max}}(f)$ are both constants. By filling in their values and calculating, the drop-off factor can be simplified as seen in Equation 3.50. From this simplification, the Big-M value of 5 is found, which multiplied by the value of 1.5 from $M_{\mathrm{C-rate}}$ gives the upper bound of 7.5 for the auxiliary variables.

$$X_{\mathrm{dropoff}}[f,t] = \frac{1}{1 - SoC_{\mathrm{tran}}(f)} \cdot (1 - \frac{SoC[f,t]}{SoC_{\mathrm{max}}(f)}) \tag{3.49}$$

$$X_{\mathrm{dropoff}}[f,t] = 5 \cdot (1 - SoC[f,t]) \tag{3.50}$$

In this part, the constraints are discussed that linearize the CPCV charging profile. There are several groups of constraints working together to achieve this, and will be discussed with their relevant parts.

Equations (3.51), (3.52), and (3.53) work together to define the $\delta_{\mathrm{CP}}^{\mathrm{ch}}[f,t]$ variable which is only 1 when the charging profile is in the CP phase *and* charging. It ensures that the CP power is only applied when and aircraft is charging and in the CP phase. It is the linearization of Equation 3.54.

$$\delta_{\mathrm{CP}}^{\mathrm{ch}}[f,t] \leq 1 - \delta_{\mathrm{CV}}[f,t] \quad \forall f \in F_{active}, \forall t \in D_{ch}(f) \tag{3.51}$$

$$\delta_{\mathrm{CP}}^{\mathrm{ch}}[f,t] \leq \delta_{\mathrm{ch}}[f,t] \quad \forall f \in F_{active}, \forall t \in D_{ch}(f) \tag{3.52}$$

$$\delta_{\mathrm{CP}}^{\mathrm{ch}}[f,t] \geq (1 - \delta_{\mathrm{CV}}[f,t]) + (\delta_{\mathrm{ch}}[f,t] - 1) \quad \forall f \in F_{active}, \forall t \in D_{ch}(f) \tag{3.53}$$

$$\delta_{\mathrm{CP}}^{\mathrm{ch}}[f,t] = (1 - \delta_{\mathrm{CV}}[f,t]) \cdot \delta_{\mathrm{ch}}[f,t] \quad \forall f \in F_{active}, \forall t \in D_{ch}(f) \tag{3.54}$$

Similarly, Equations (3.55), (3.56), and (3.57) work together to define the $\delta_{\mathrm{CV}}^{\mathrm{ch}}[f,t]$ variable which is only 1 when the charging profile is in the CV phase *and* charging. It is the linearization of (3.58)

$$\delta_{\mathrm{CV}}^{\mathrm{ch}}[f,t] \leq \delta_{\mathrm{CV}}[f,t] \quad \forall f \in F_{active}, \forall t \in D_{ch}(f) \tag{3.55}$$

$$\delta_{\mathrm{CV}}^{\mathrm{ch}}[f,t] \leq \delta_{\mathrm{ch}}[f,t] \quad \forall f \in F_{active}, \forall t \in D_{ch}(f) \tag{3.56}$$

$$\delta_{\mathrm{CV}}^{\mathrm{ch}}[f,t] \geq \delta_{\mathrm{CV}}[f,t] + (\delta_{\mathrm{ch}}[f,t] - 1) \quad \forall f \in F_{active}, \forall t \in D_{ch}(f) \tag{3.57}$$

$$\delta_{\mathrm{CV}}^{\mathrm{ch}}[f,t] = \delta_{\mathrm{CV}}[f,t] \cdot \delta_{\mathrm{ch}}[f,t] \quad \forall f \in F_{active}, \forall t \in D_{ch}(f) \tag{3.58}$$

Next, Equations (3.59) - (3.63) linearize the CP phase power.
The auxiliary variable $P^{\text{aux}}_{\text{CP}}[f,t]$ represents the C-rate when the CP phase is active and charging as seen in Equation 3.64. It uses Big-M values to linearize the conditional logic and computes the final CP power used by the system.

$$P^{\text{aux}}_{\text{CP}}[f,t] \leq R^{\text{ch}}_{\text{aircraft}}(f) \quad \forall f \in F_{active}, \forall t \in D_{ch}(f) \tag{3.59}$$

$$P^{\text{aux}}_{\text{CP}}[f,t] \geq R^{\text{ch}}_{\text{aircraft}}(f) - M_{\text{C-rate}} \cdot (1 - \delta^{\text{ch}}_{\text{CP}}[f,t]) \quad \forall f \in F_{active}, \forall t \in D_{ch}(f) \tag{3.60}$$

$$P^{\text{aux}}_{\text{CP}}[f,t] \leq M_{\text{C-rate}} \cdot \delta^{\text{ch}}_{\text{CP}}[f,t] \quad \forall f \in F_{active}, \forall t \in D_{ch}(f) \tag{3.61}$$

$$P^{\text{ch}}_{\text{CP}}[f,t] \leq P^{\text{aux}}_{\text{CP}}[f,t] B_{\text{cap}}(f) \quad \forall f \in F_{active}, \forall t \in D_{ch}(f) \tag{3.62}$$

$$P^{\text{ch}}_{\text{CP}}[f,t] \geq P^{\text{aux}}_{\text{CP}}[f,t] B_{\text{cap}}(f) - M_{\text{C-rate}} B_{\text{cap}}(f) \cdot (1 - \delta^{\text{ch}}_{\text{CP}}[f,t]) \quad \forall f \in F_{active}, \forall t \in D_{ch}(f) \tag{3.63}$$

$$P^{\text{aux}}_{\text{CP}}[f,t] = R^{\text{ch}}_{\text{aircraft}}(f) \delta^{\text{ch}}_{\text{CP}}[f,t] \quad \forall f \in F_{active}, \forall t \in D_{ch}(f) \tag{3.64}$$

For the linearization of the more complicated CV phase, Equations (3.65) - (3.71) are put in place for Equation 3.72. The $X^{\text{dropoff}}_{\text{C-rate}}[f,t]$ auxiliary variable approximates the product of $1.5 \cdot X_{\text{dropoff}}[f,t]$, which is bounded to ensure feasible values. The $P^{\text{base}}_{\text{CV}}[f,t]$ auxiliary variable linearizes the product between $X^{\text{dropoff}}_{\text{C-rate}}[f,t]$ and $\delta^{\text{ch}}_{\text{CV}}[f,t]$ using Big-M values to set the CV power to zero when not in the CV phase or not charging. Finally, $P^{\text{ch}}_{\text{CP}}[f,t]$ computes the CV power by scaling $P^{\text{base}}_{\text{CV}}[f,t]$ with the aircraft's battery capacity.

$$X^{\text{dropoff}}_{\text{C-rate}}[f,t] \leq M_{\text{C-rate}} X_{\text{dropoff}}[f,t] \quad \forall f \in F_{active}, \forall t \in D_{ch}(f) \tag{3.65}$$

$$X^{\text{dropoff}}_{\text{C-rate}}[f,t] \leq M_{\text{dropoff}} R^{\text{ch}}_{\text{aircraft}}(f) \quad \forall f \in F_{active}, \forall t \in D_{ch}(f) \tag{3.66}$$

$$X^{\text{dropoff}}_{\text{C-rate}}[f,t] \geq M_{\text{C-rate}} X_{\text{dropoff}}[f,t] + M_{\text{dropoff}} R^{\text{ch}}_{\text{aircraft}}(f) - M_{\text{dropoff}} M_{\text{C-rate}} \quad \forall f \in F_{active}, \forall t \in D_{ch}(f) \tag{3.67}$$

$$P^{\text{base}}_{\text{CV}}[f,t] \leq X^{\text{dropoff}}_{\text{C-rate}}[f,t] \quad \forall f \in F_{active}, \forall t \in D_{ch}(f) \tag{3.68}$$

$$P^{\text{base}}_{\text{CV}}[f,t] \leq M_{\text{dropoff}} M_{\text{C-rate}} \cdot \delta^{\text{ch}}_{\text{CV}}[f,t] \quad \forall f \in F_{active}, \forall t \in D_{ch}(f) \tag{3.69}$$

$$P^{\text{base}}_{\text{CV}}[f,t] \geq X^{\text{dropoff}}_{\text{C-rate}}[f,t] - M_{\text{dropoff}} M_{\text{C-rate}} \cdot (1 - \delta^{\text{ch}}_{\text{CV}}[f,t]) \quad \forall f \in F_{active}, \forall t \in D_{ch}(f) \tag{3.70}$$

$$P^{\text{ch}}_{\text{CV}}[f,t] = B_{\text{cap}}(f) P^{\text{base}}_{\text{CV}}[f,t] \quad \forall f \in F_{active}, \forall t \in D_{ch}(f) \tag{3.71}$$

$$P^{\text{ch}}_{\text{CV}}[f,t] = 5 \cdot R^{\text{ch}}_{\text{aircraft}}(f) B_{\text{cap}}(f) \cdot (1 - SoC[f,t]) \quad \forall f \in F_{active}, \forall t \in D_{ch}(f) \tag{3.72}$$

Finally, Equations (3.73)-(3.76) are put in place to enforce the correct transition between the CP and CV phases at the $SoC_{\text{tran}}(f)$ and make the CP and CV powers mutually exclusive. They make sure that $P^{\text{ch}}_{\text{CV}}[f,t]$ is zero when the CP phase is active, and vice versa for $P^{\text{ch}}_{\text{CP}}[f,t]$.

$$SoC[f,t] \leq SoC_{\text{tran}}(f) \cdot \delta_{\text{CV}}[f,t] \quad \forall f \in F_{active}, \forall t \in D_{ch}(f) \tag{3.73}$$

$$SoC[f,t] - SoC_{\text{tran}}(f) \leq (1 - SoC_{\text{tran}}(f)) \cdot \delta_{\text{CV}}[f,t] \quad \forall f \in F_{active}, \forall t \in D_{ch}(f) \tag{3.74}$$

$$P^{\text{ch}}_{\text{CP}}[f,t] \leq M_{\text{C-rate}} B_{\text{cap}}(f) \cdot (1 - \delta_{\text{CV}}[f,t]) \quad \forall f \in F_{active}, \forall t \in D_{ch}(f) \tag{3.75}$$

$$P^{\text{ch}}_{\text{CV}}[f,t] \leq M_{\text{C-rate}} B_{\text{cap}}(f) \cdot \delta^{\text{ch}}_{\text{CV}}[f,t] \quad \forall f \in F_{active}, \forall t \in D_{ch}(f) \tag{3.76}$$

4

Results

Now that the objective function and constraints are in place, the optimization model is ready to start solving. *Gurobi* is used as the linear solver on the *Pyomo* model that was written in *Python*. In this chapter, four one-week scenarios are considered in the following months: October, January, April, and July 2019. A month from each season of the year was chosen to account for seasonal differences in the PV system and the differences in flight counts within each category.

4.1. Three-Step Solve

A three-step solve was chosen to obtain the desired results. Due to the CPCV constraints and how their constraints have been made linear, a small relaxation became present in their logic. Because of this, the CV power would at times spike above the limit set by the CP power. To account for this, the second run is used to determine the charging C-rates for each flight in the simulation. Afterwards, these C-rates are fixed, and the constraint for the CV power is simplified as it now only accounts for the SoC during charging. Now, the CPCV charging profile is correct for every flight where it is necessary. Figure 4.1 shows a charging profile from the simulation output.

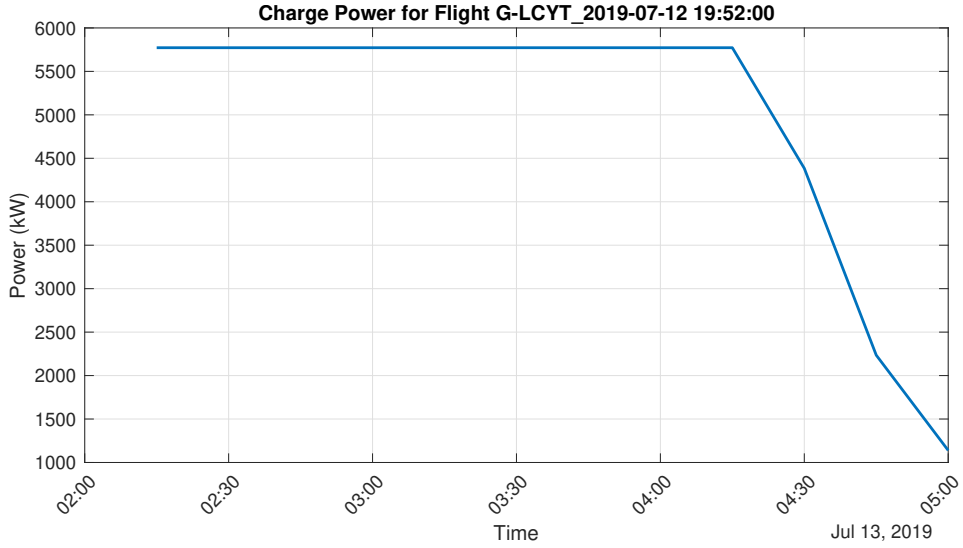

Figure 4.1: CPCV charging curve in optimization

The second reason a three-step approach was chosen was due to the sizing of the BESS. As there is no cost associated with the BESS sizing, as it is not included in the operational cost, the model always starts with the set upper limit of 20 MWh. In the first solve, the program looks at the highest discharged

power from the BESS, which is divided by 2 to account for maximum C-rate and to size the BESS for the second and third solve. Additionally, this new size is rounded to the nearest multiple of 500 kWh, with another 500 kWh added as a buffer and to reduce the solving time.

In general, this means that the BESS sizing starts as a variable in the first solve, and becomes a parameter in the other two. The C-rates are variable during the first two solves, and become a parameter in the last solve.

4.2. Turnaround Times and Cancellations

The following sections present the simulation results that were conducted for the different weeks will be discussed. Each month uses the same week to run the simulation, spanning from the 10^{th}-18^{th} of that month. First, an analysis of delays and cancellations will be performed for each month. Then, the graphs regarding power flows, BESS SoC, and BESS degradation will be discussed together to support the results of the flight scheduling. For clarity, the grid import and export powers are combined in the power graphs, as well as the BESS charge and discharge powers.

January

In the middle of winter, solar irradiance and sunlight hours are low, drastically reducing the power available from the PV installation. With a relatively high flight count, especially for commercial aviation, charging power peaks will be quite high. In Figures (4.2) - (4.4) provide a detailed overview is given into the turnaround times for each category over the simulation period. Additionally, Figure 4.5 provides a detailed insight in the delay times of the flights. In this particular week, there were no business flights.

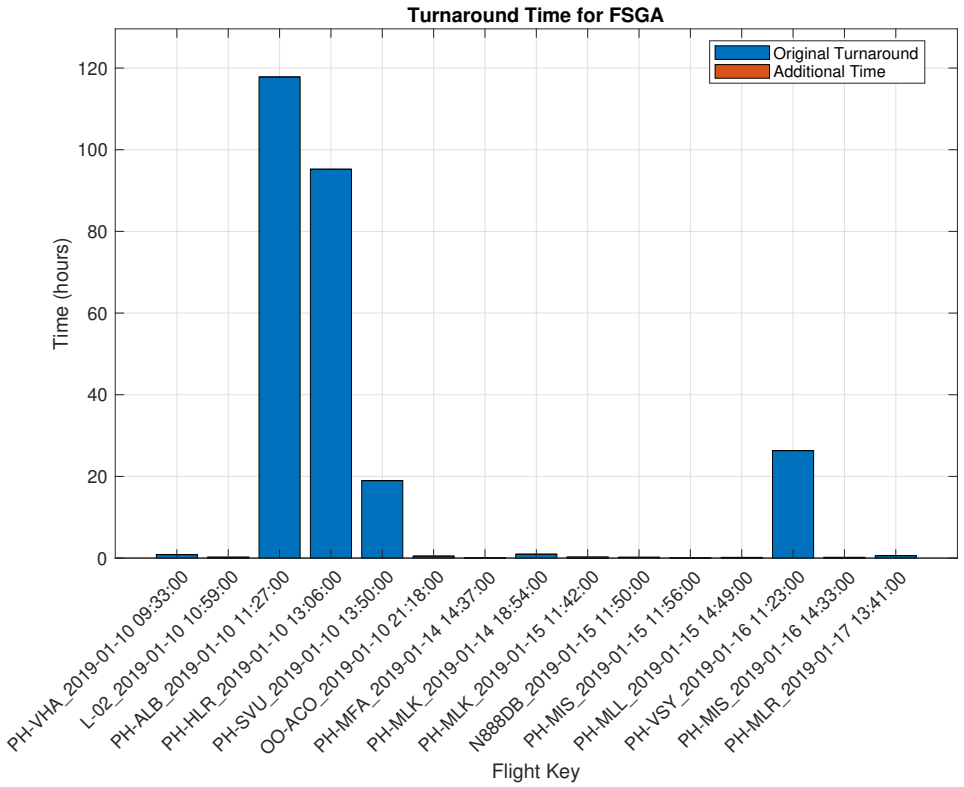

Figure 4.2: FSGA Turnaround times for January

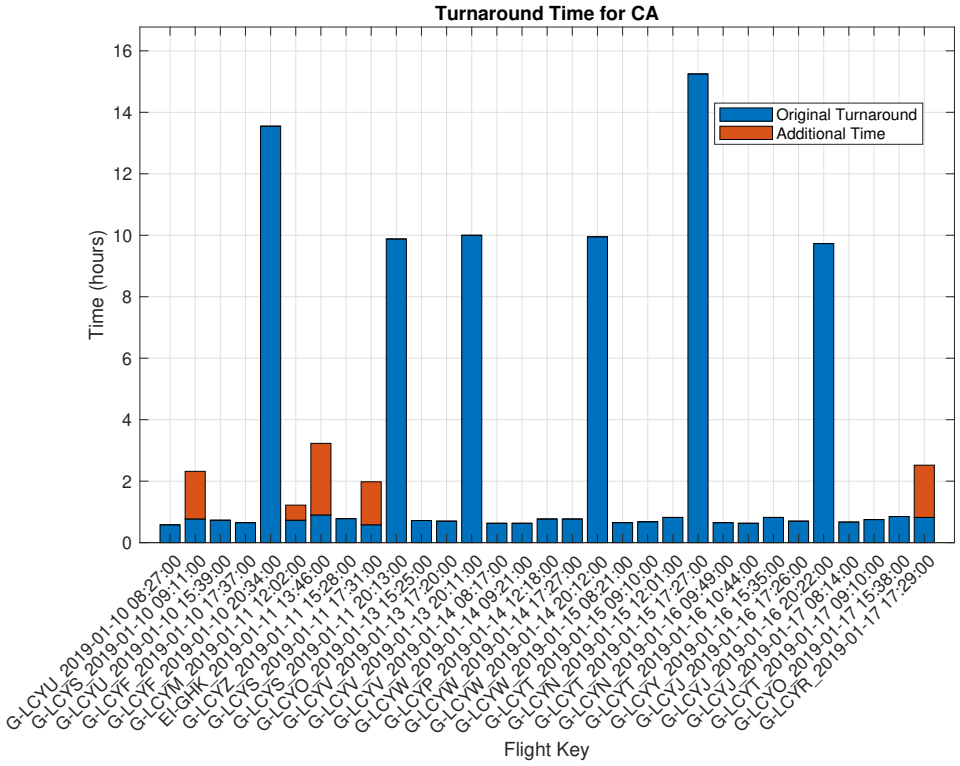

Figure 4.3: CA Turnaround times for January

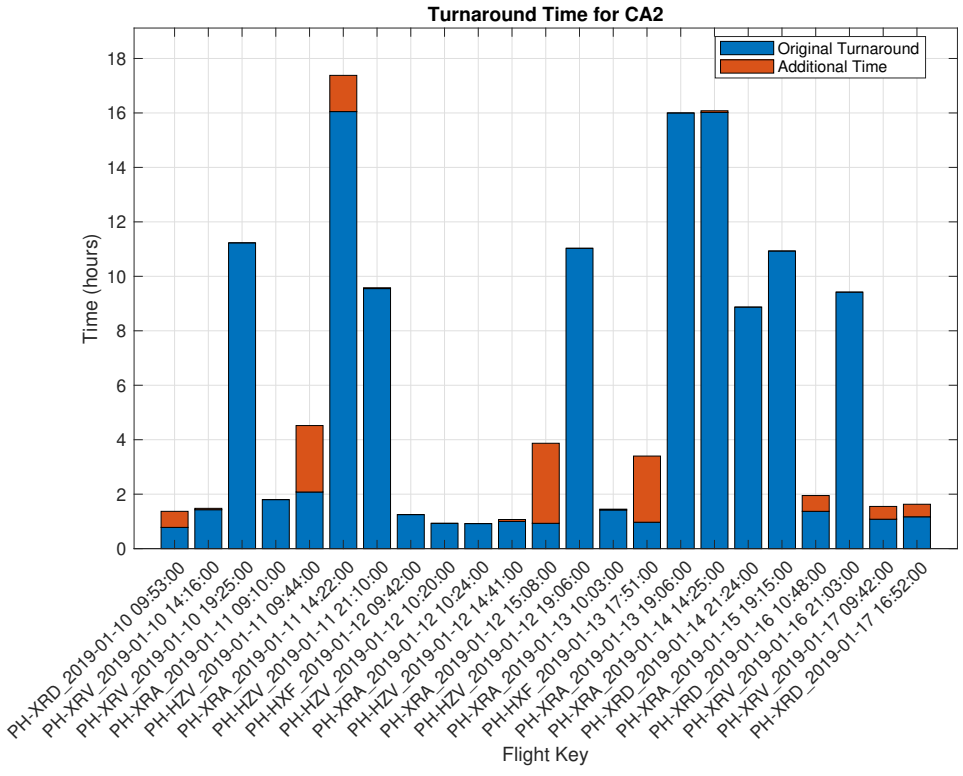

Figure 4.4: CA2 Turnaround times for January

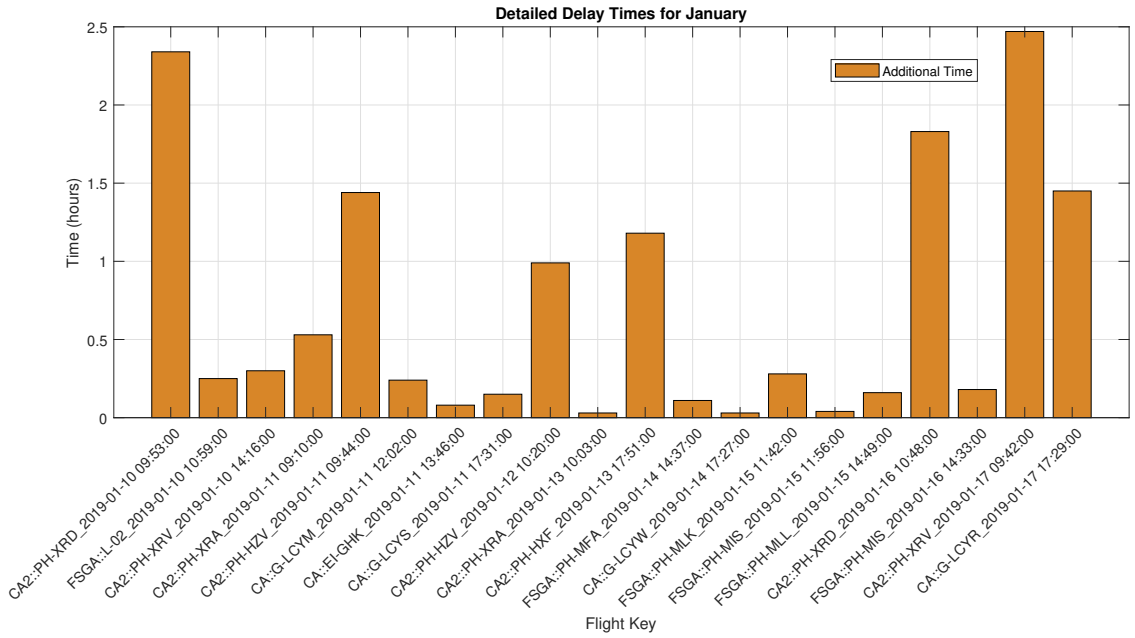

Figure 4.5: Detailed Delay Times January

Table 4.1 breaks down the flight results for January. Here, it can be seen that there are almost as many CA2 flights as CA flights, which has a significant impact on power needs. Due to more large flights leaving for close destinations in winter, an increase in CA2 flights can be explained. In addition, there is a total delay time of 14 hours during the week, with three canceled flights in the CA2 category. This could be explained by the flight schedule on January 12, where three different CA2 flights arrived at the airport in a span of 40 minutes, canceling two of the flights. With their high energy demands and the delays of other flights, three flights in total had to be canceled that day because their energy demand could not be met within the allocated turnaround and its extension interval.

Table 4.1: Flight results for January

Category	Count	Delayed Flights	Delay Time (min)	Average Delay (min)	Canceled Flights
FSGA	15	6	61.2	10.2	0
BA	0	0	0	0	0
CA	31	5	112.2	22.44	0
CA2	23	9	666.4	74	3
Total	69	20	844.8	44.24	3

The 45-minute average delay in January reflects the high power demand of the large number of commercial aviation flights and low power availability from the PV system. Additionally, the delay times of the FSGA category can be explained by their original turnaround times. For some flights, this can be in the range of 5-10 minutes, which will always be too little time to charge the aircraft with the imposed maximum C-rates. The impact of these delays on power flows and BESS performance is explored in Sections (4.3)-(4.7).

April

The simulation for April 2019 had a very sunny week, with a lot of PV power available for the system. With less flights of the CA2 category, a smaller peak charging power is present. Figures (4.12) - (4.8) again give a detailed overview into the turnaround times for each category. Here, it can be seen that even when a delay is present, it is a short one.

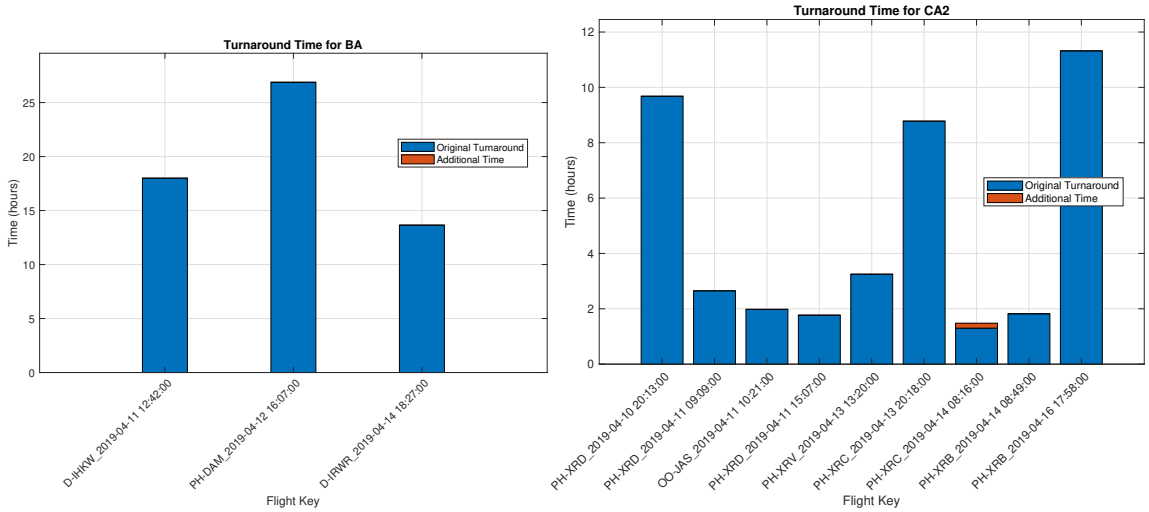

(a) BA Turnaround times

(b) CA2 Turnaround times

Figure 4.6: BA and CA2 Turnaround times for April

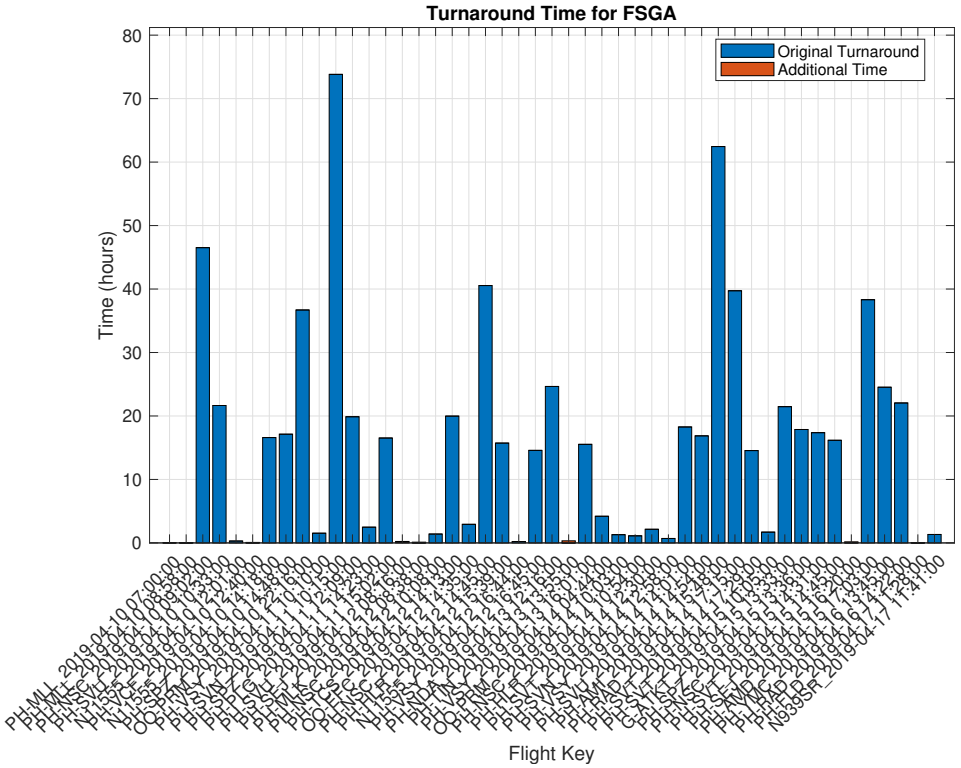

Figure 4.7: FSGA Turnaround times for April

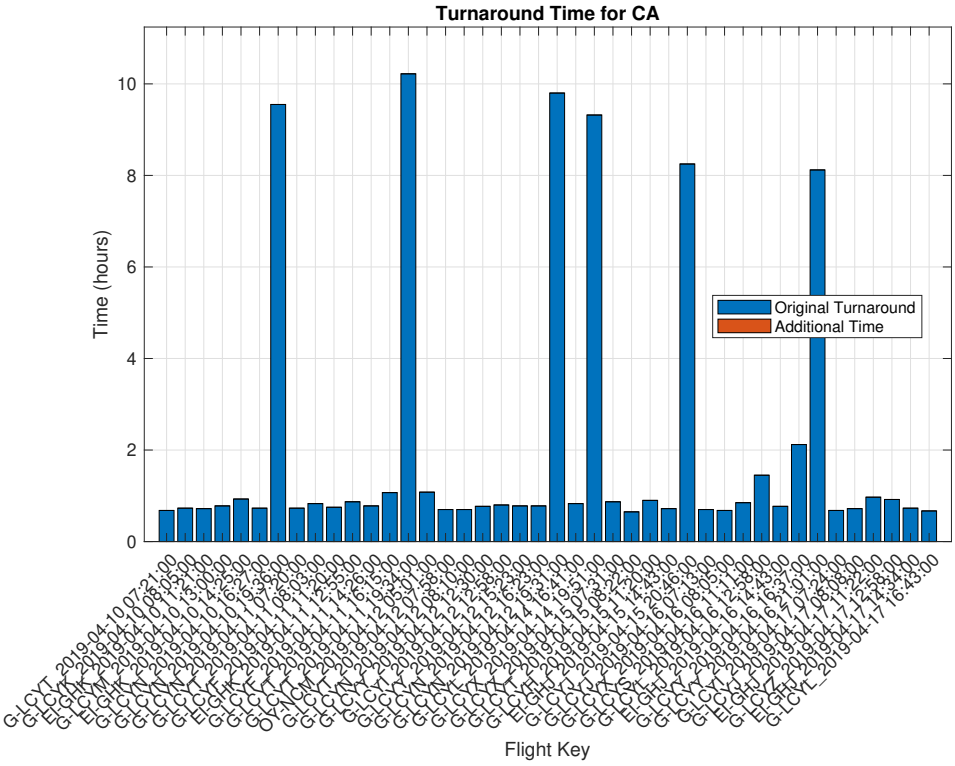

Figure 4.8: CA Turnaround times for April

Table 4.2 breaks down the flight results for April. Here, it becomes clear that the number of CA2 flights is quite low compared to the CA flights, reducing the overall impact on the charging power. With more flights leaving to more distant destinations, the CA2 category has a lower number of flights. In total, only an hour of delay time was added to allow the flight schedule to stand. Each flight received the full amount of energy needed to fulfill its next mission, which lead to no canceled flights.

Table 4.2: Flight results for April

Category	Count	Delayed Flights	Delay Time (min)	Average Delay (min)	Canceled Flights
FSGA	47	7	44.4	6.34	0
BA	3	0	0	0	0
CA	42	0	0	0	0
CA2	9	1	11	11	0
Total	101	8	55.4	6.92	0

With only an average delay time of 7 minutes, it can be seen that the impact and performance of the PV park on the system is crucial in reducing charge power peaks. In addition to this, the longer difference in arrival times between CA flights allows the system to deliver the energy without imposing long delay times.

July

In the middle of summer, PV generation is at its yearly peak. With a high irradiance and more hours of sun, the PV park will be able to assist the system in a consistent way. In July, there are no eligible CA2 flights as long-haul aircraft are used to serve distant sunny routes which are too far for the electrical equivalent.

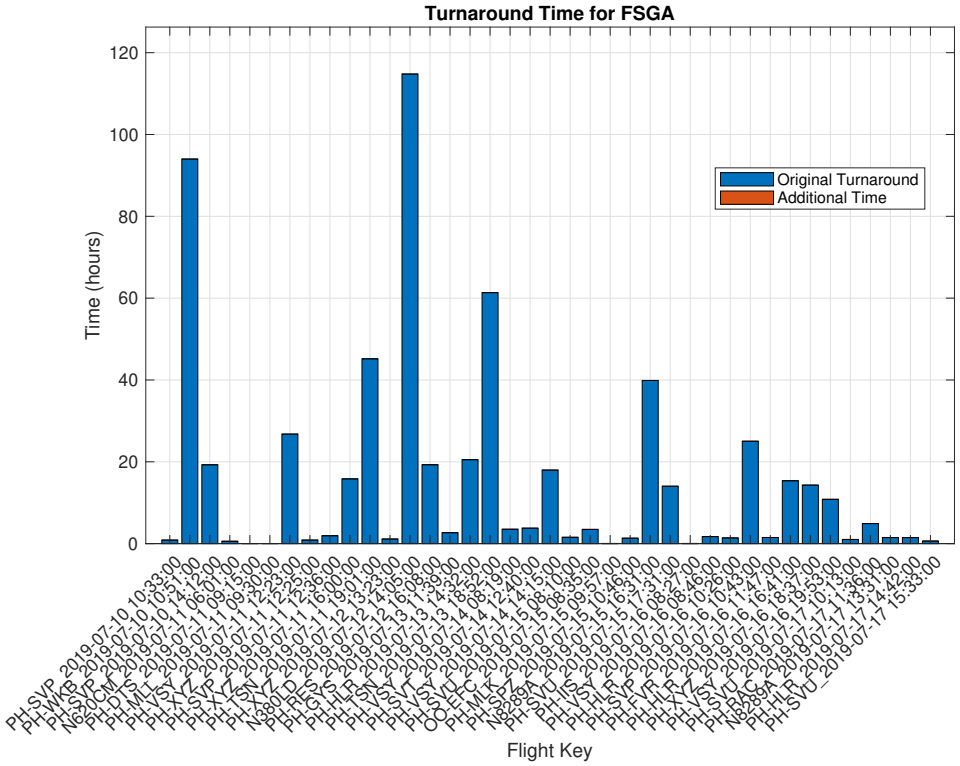

Figure 4.9: FSGA Turnaround times for July

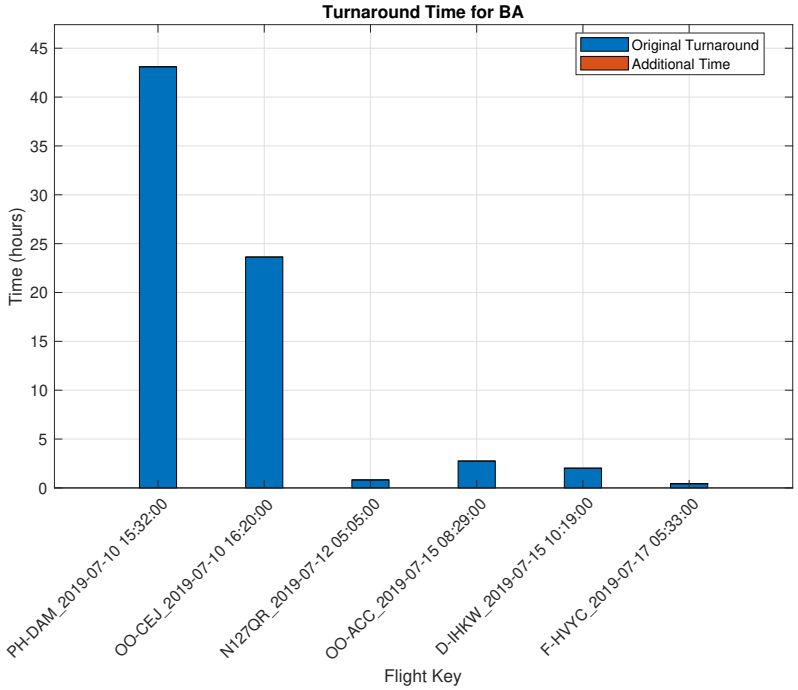

Figure 4.10: BA Turnaround times for July

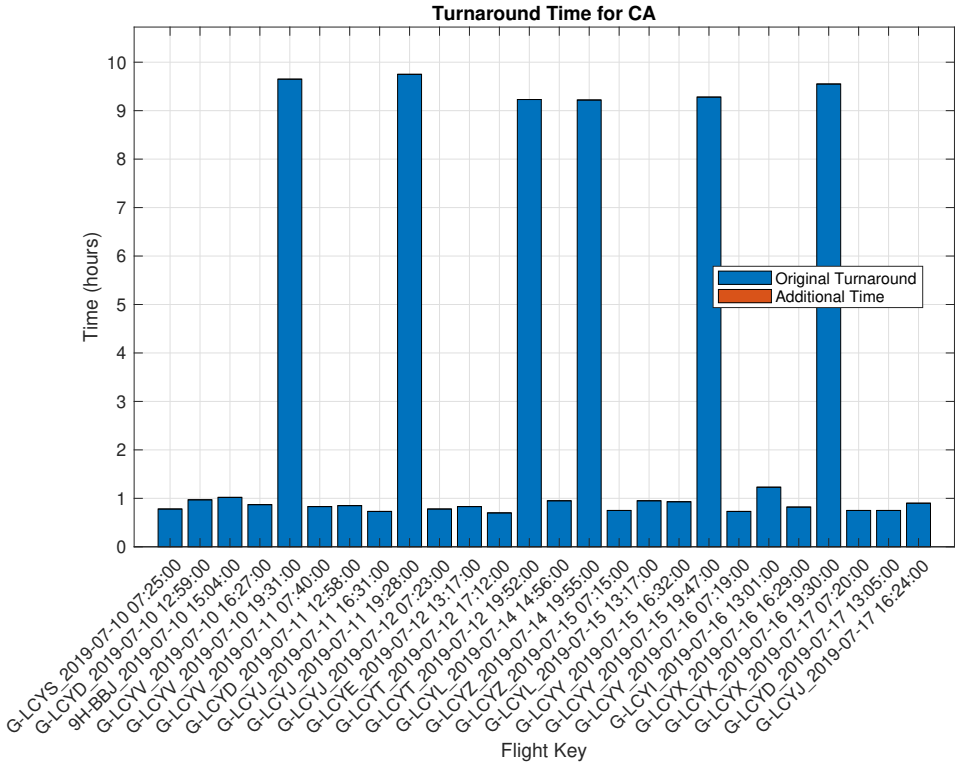

Figure 4.11: CA Turnaround times for July

In Table 4.2 the flight results are summarized for July. Here, it is seen that there are no CA2 flights during the simulation week which lowers the charging peaks. In total, only four minutes of delay time was added to allow the flight schedule to stand, in the FSGA and BA categories. These delays are as good as negligent. Each flight received the full amount of energy needed to fulfill its next mission, which lead to no canceled flights.

Table 4.3: Flight results for July

Category	Count	Delayed Flights	Delay Time (min)	Average Delay (min)	Canceled Flights
FSGA	39	2	3.6	1.8	0
BA	6	1	1.2	1.2	0
CA	26	0	0	0	0
CA2	0	0	0	0	0
Total	71	3	4.8	1.4	0

In addition to the high PV power, it can be seen that the shortage of CA2 flights allow the system to keep delay times to a minimum.

October

In October, the available PV power becomes less and less as fall and winter are coming into the picture. The overall flight demand is slowly shifting back to incorporate more CA2 flights back into the schedule. During this week, the increase of CA2 flights is less noticeable, as only one is present.

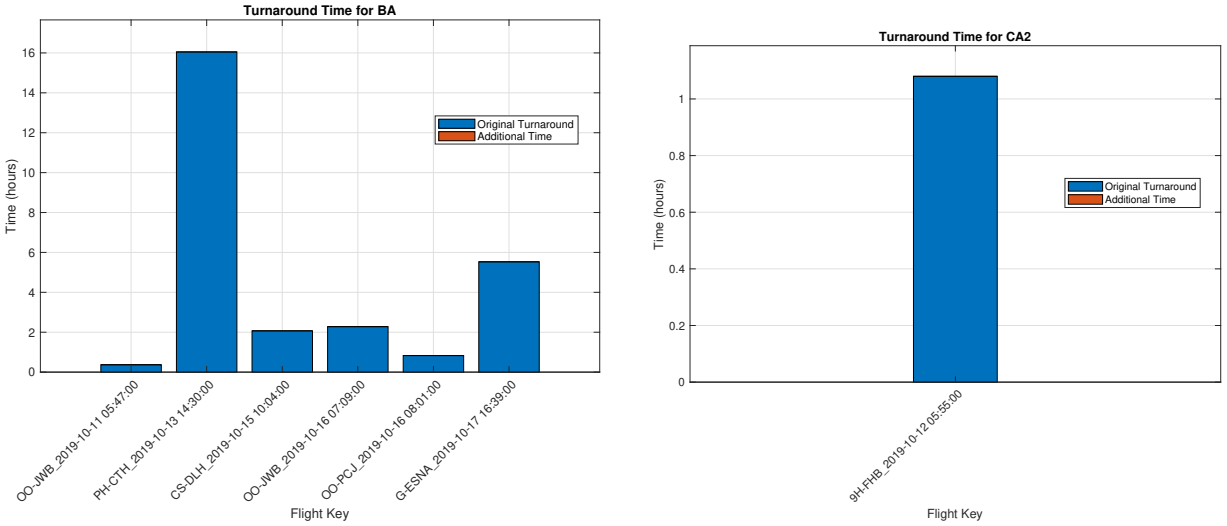

(a) BA Turnaround times

(b) CA2 Turnaround times

Figure 4.12: BA and CA2 Turnaround times for October

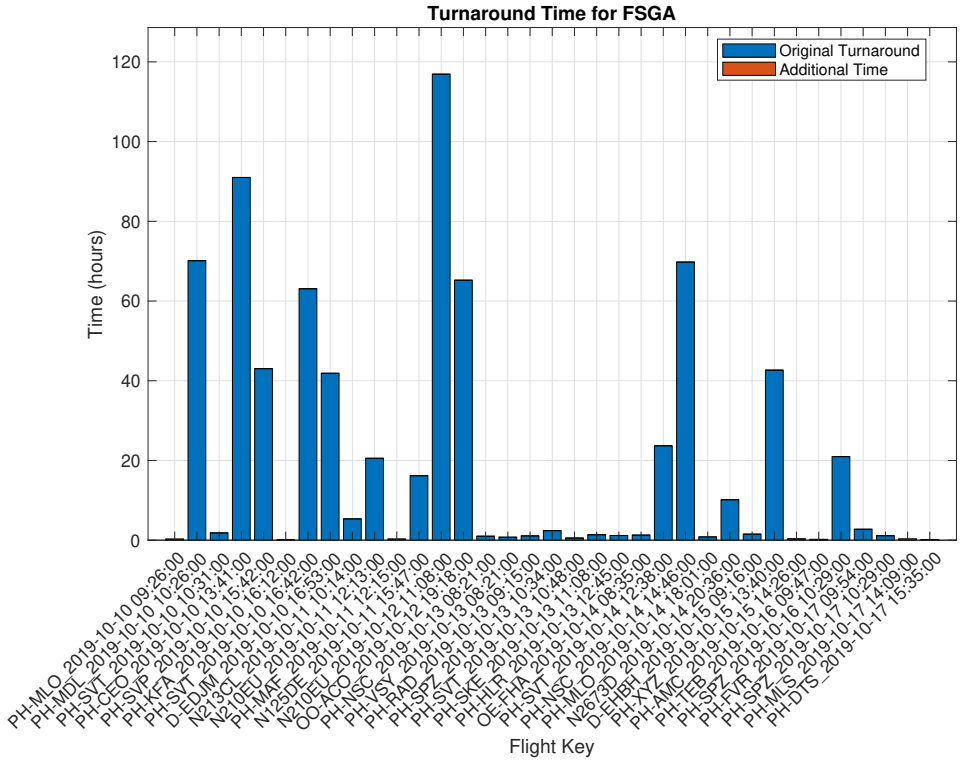

Figure 4.13: FSGA Turnaround times for October

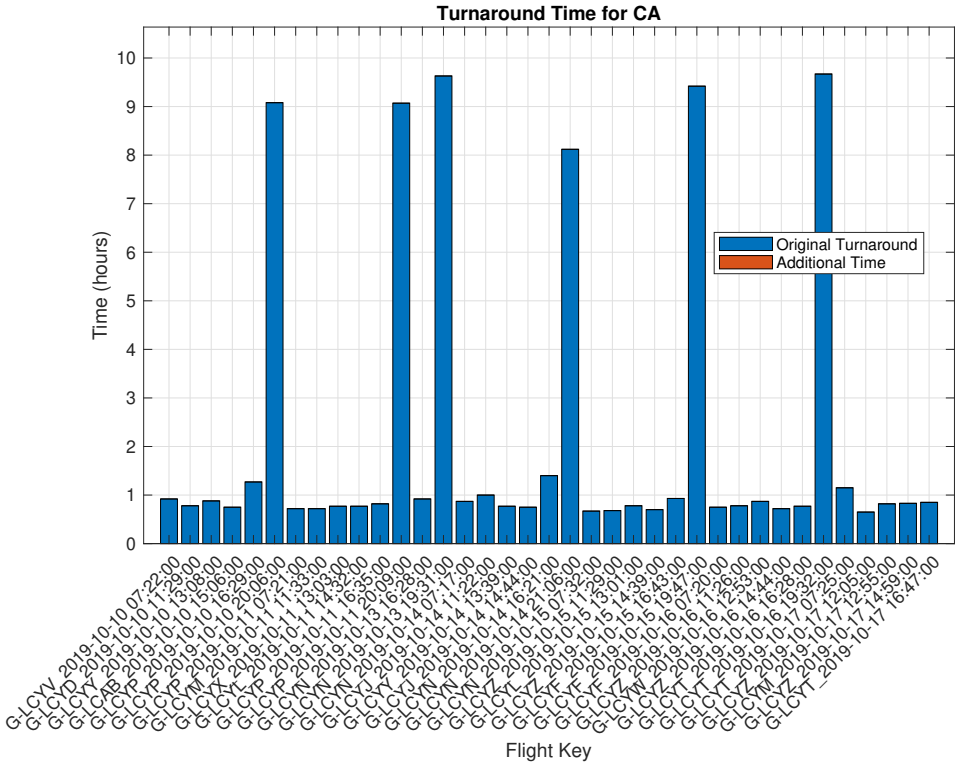

Figure 4.14: CA Turnaround times for October

In Table 4.4, it can be seen that the flight count is comparable to the ones in July. With only a total delay of one hour, all of which are imposed on FSGA flights, the system can handle the provided flight schedule well. The CA and CA2 flights have a manageable time between arrivals, removing the need for delays for those categories.

Table 4.4: Flight results for October

Category	Count	Delayed Flights	Delay Time (min)	Average Delay (min)	Canceled Flights
FSGA	35	5	59.4	11.88	0
BA	6	0	0	0	0
CA	37	0	0	0	0
CA2	1	0	0	0	0
Total	79	5	59.4	11.88	0

4.3. Power Curves

The following section presents an analysis of the power curves across the different simulation scenarios. Here, it will show the power interactions between grid power, BESS operations, and PV generation to meet the demands of the airport and the flight charging. The curves will provide insight into the seasonal variations of the PV generation, as well as the variations in charging power demands and its constraints on the system and how the optimization manages power flows in these scenarios.

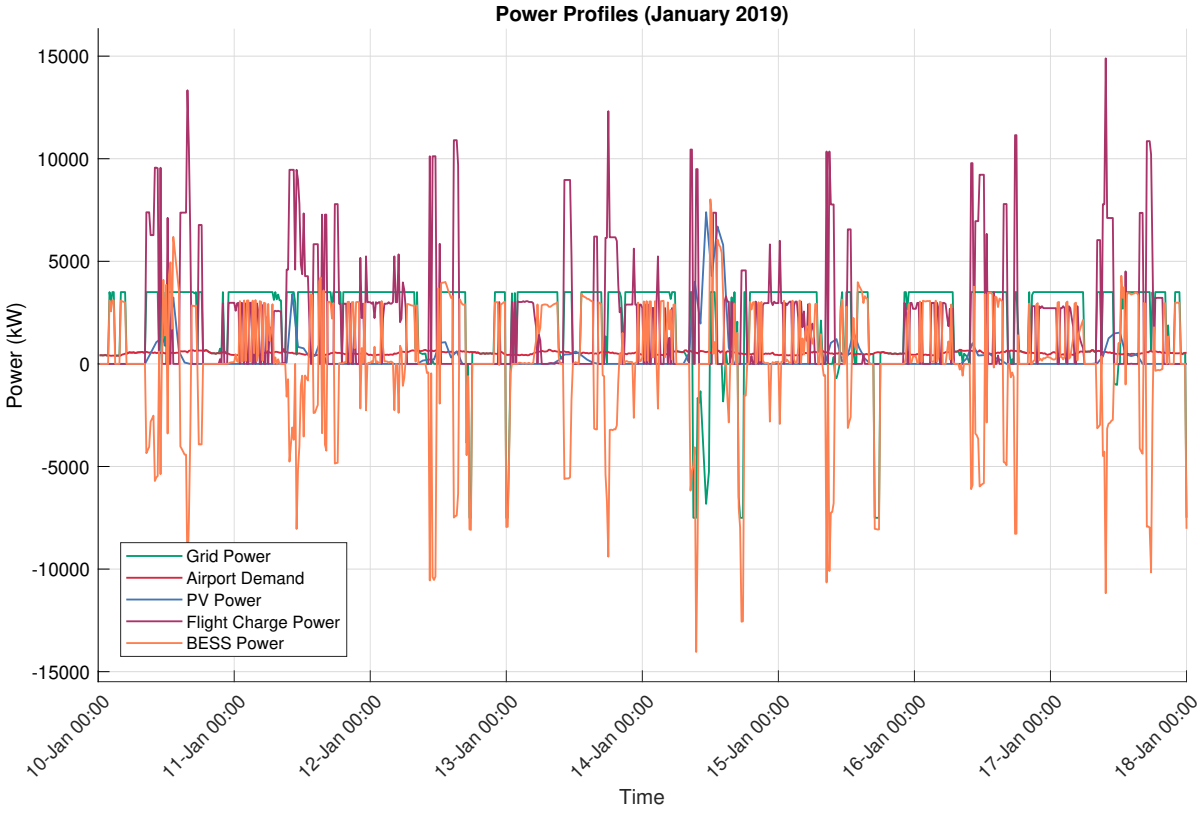

Figure 4.15: Power curves for January

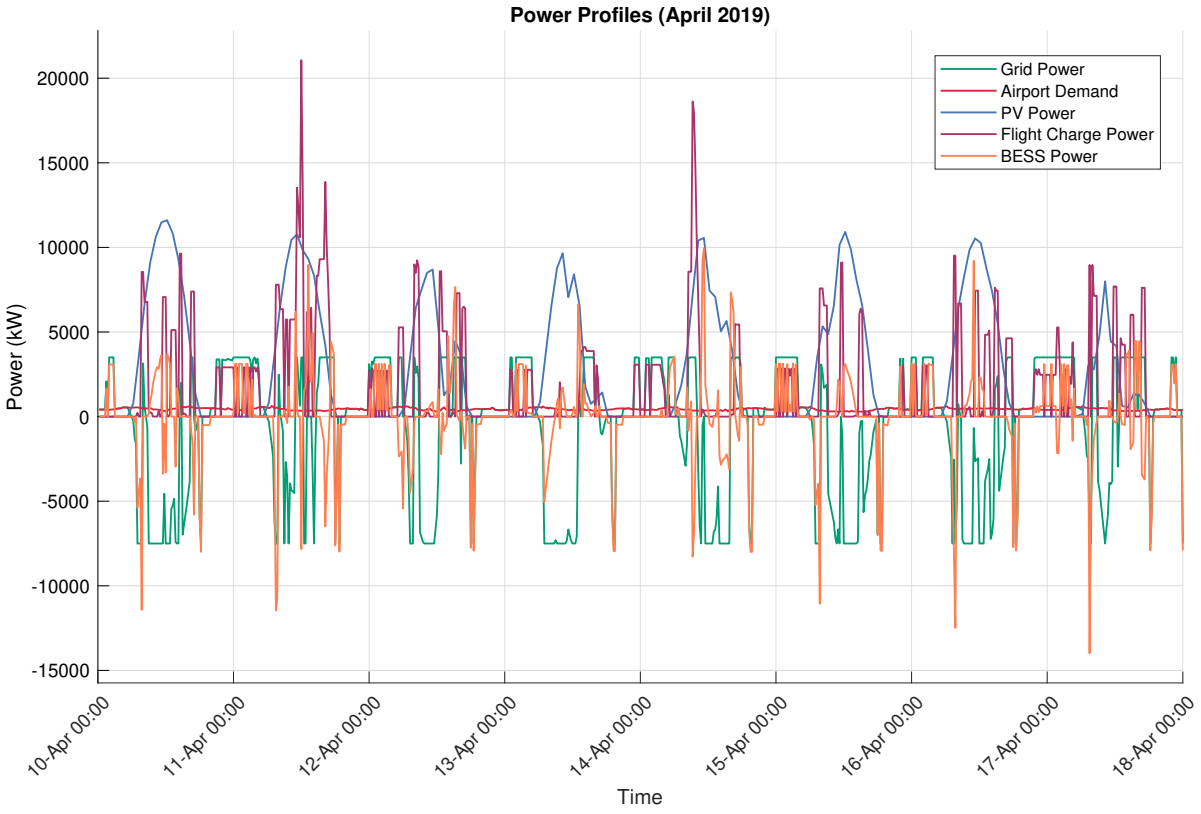

Figure 4.16: Power curves for April

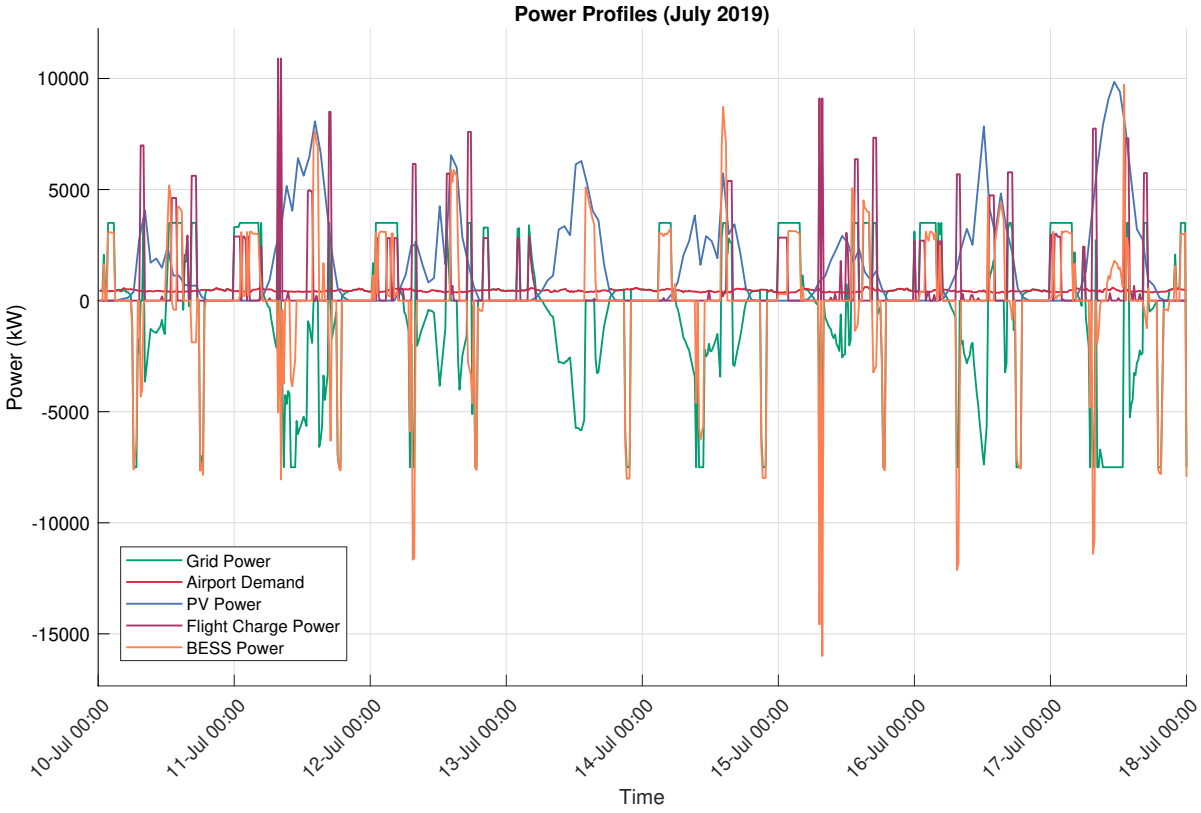

Figure 4.17: Power curves for July

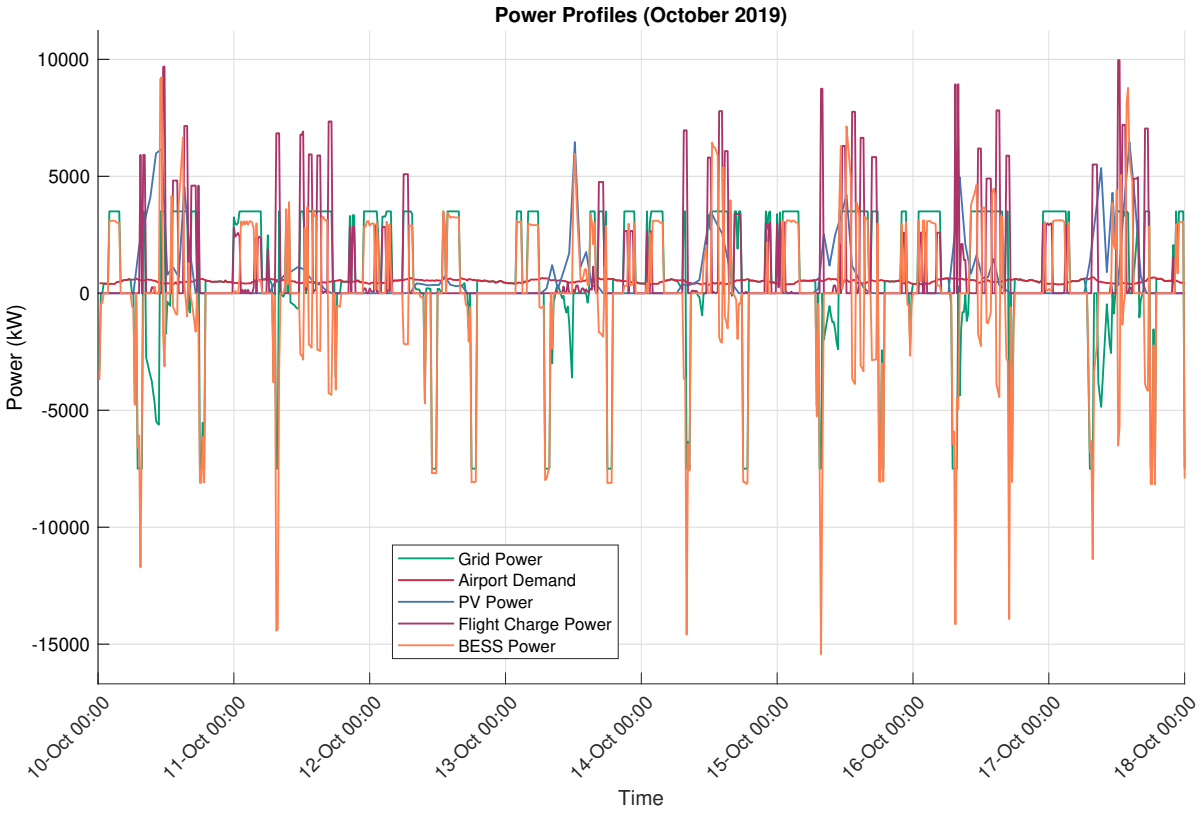

Figure 4.18: Power curves for October

PV Generation

PV generation shows significant seasonal variations across the simulation weeks. January's PV power remains low, staying well below 5 MW, except on the more sunny January 14, where it could also export some of its power to the grid to make up some of the cost. With its low contribution to the power demand, there is heavier reliance on grid import and BESS energy. April shows the highest PV contribution of all simulations, where it steadily provides around 10 MW to the system to assist in the high charging demands. On multiple occasions, it exports the full 7.5 MW limit to the grid when there is an abundance of power. July has slightly lower PV generation, which could be due to worse weather conditions. Here, it provides between 4-10 MW of power to the system, depending on the day. With lowered charging demands due to lack of CA2 flights, it is able to provide enough energy, while also exporting power back to the grid. This is also visible in the PV generation for October.
The PV power trends influence grid and BESS reliance. In the darker months of January and October, more grid power is used with larger BESS power peaks, showing the need for extra BESS storage or a larger grid connection. In contrast, sunnier months April and July are less reliant on grid power and BESS power peaks.

Flight Charging Power

The flight charging power shows large variations in peak magnitude and frequency between the simulations. January, with a large number of CA and CA2 flights, shows several high demand peaks surpassing 12-13 MW at the same time which contributes to the high delay times. April, with a lower number of CA2 flights has two high peaks exceeding 15 and 20 MW and otherwise staying below a charging demand of 10 MW. The increased PV generation alleviates large amounts of power from these peaks. With lower PV generation in July, the charging peaks are between 5-10 MW in magnitude due to the lack of CA2 flights. In October, due to the evenly spread arrival times of flights, the charging peaks only exceed 10 MW once, mostly staying under 8 MW during the rest of the simulation.

BESS Power

Lastly, the BESS powers show different magnitudes in the power curves. It provides an insight in the sizing of the BESS, as the maximum charge and discharge limits are bounded by their respective C-rates. In January, frequent discharge peaks of 10-15 MW can be seen, which shows the need for a large-capacity BESS to alleviate the power peaks. For April, the discharge powers have a maximum magnitude of 10-14 MW, which compared to January, the demand in April can be up to 1 MW less. However, it also utilizes the BESS to export power back to the grid to make up for some costs. In July, with its lower PV generation, the discharge powers have a maximum value of 15 MW, which in some cases is present to give power back to the grid to make revenue. Lastly, October shows peaks between 10-15 MW to compensate for the lower PV generation in the fall. Again, the system exports power from the BESS to the grid on multiple occasions to make revenue. Compared to the other colder month of January, these peaks are of the same magnitude, but differ in C-rate due to the smaller BESS size in October.

4.4. BESS SoC Curves

This section delves into the BESS SoC curves for the simulation periods. These levels reflect how the seasonal power differences and flight charging demands impact the BESS energy levels.

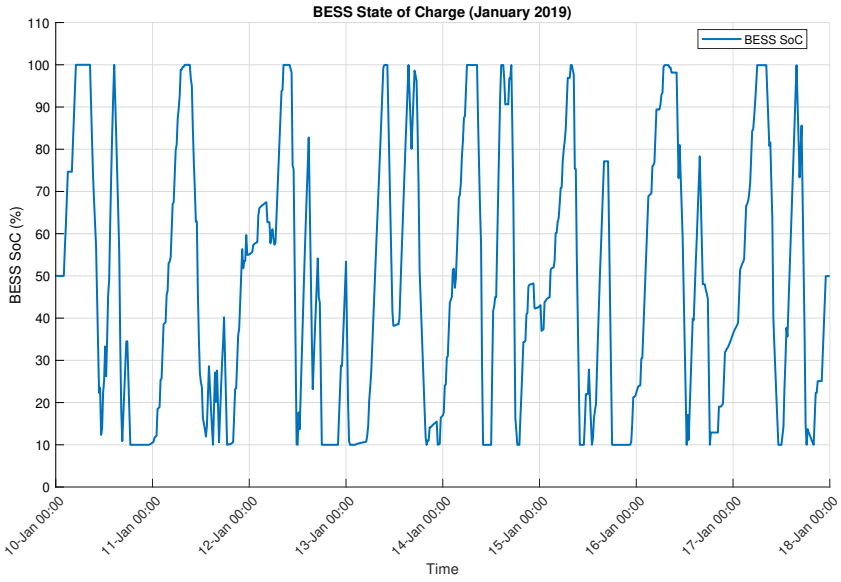

Figure 4.19: BESS SoC curve for January

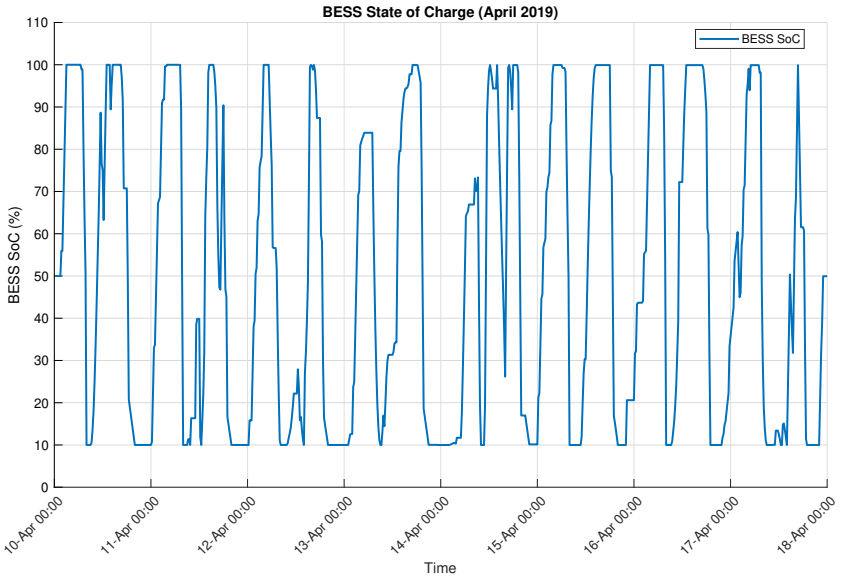

Figure 4.20: BESS SoC curve for April

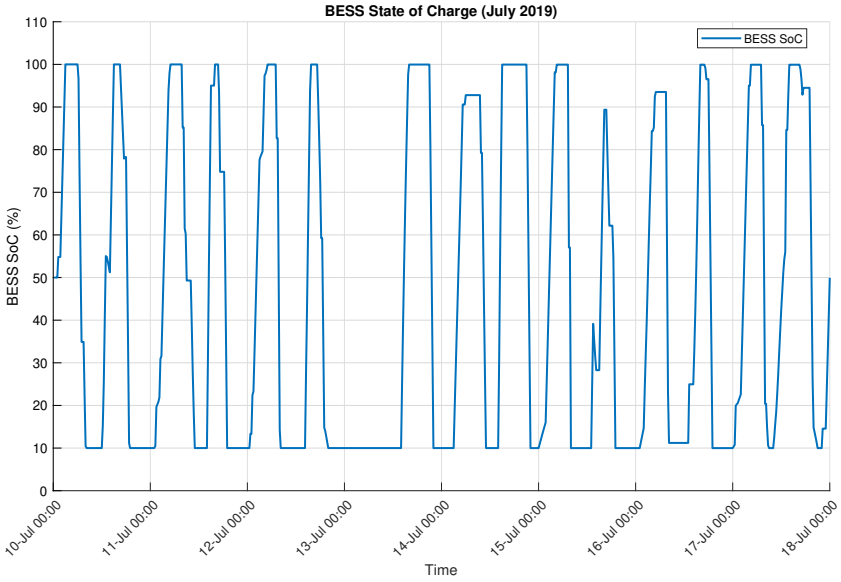

Figure 4.21: BESS SoC curve for July

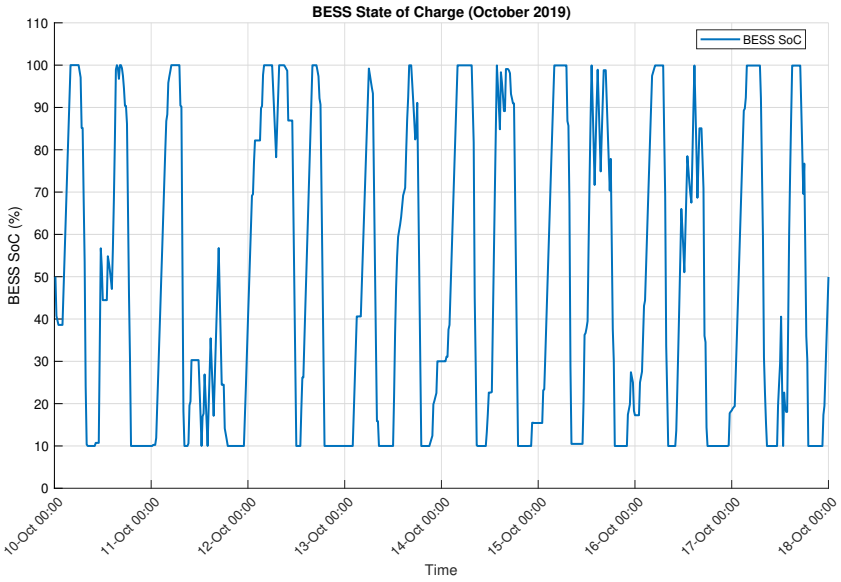

Figure 4.22: BESS SoC curve for October

For each simulation the limited SoC range of 10%-100% is fully utilized. In January, it can be seen that the SoC evolution is very irregular. Due to the high and constant flight charging demands, there is not enough power available to charge the BESS during the day. April has a smoother SoC evolution, charging the BESS when possible with grid and PV power, and discharging when flights need charging or when power is exported to the grid. July shows that the BESS goes through up to two full cycles each day. With lower charging demands, the BESS can be cycled in a more predictive way. With high PV generation and low charging demands on July 13, the optimizer chooses to utilize the extra PV power and BESS energy to export to the grid to make revenue. Lastly, October resembles January with the irregular cycling patterns. With higher charge power demands and lower PV power, the BESS is utilized more heavily throughout the simulation.

4.5. BESS Degradation Curves

This section investigates the BESS degradation curves, assessing the capacity loss over the simulation week and the influence of cycling patterns and power flows which were analyzed in section 4.3 and section 4.4. The curves will provide insight into the long-term viability of the BESS in each simulation.

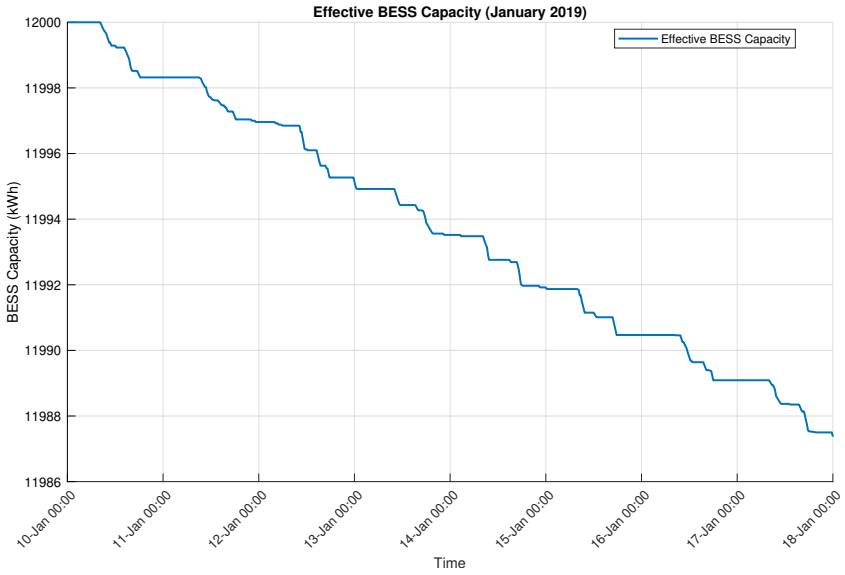

Figure 4.23: Effective BESS evolution for January

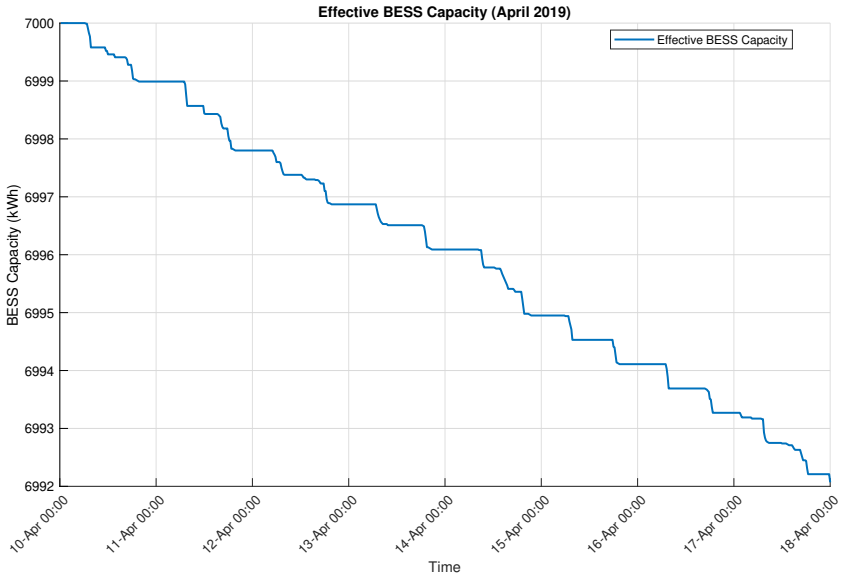

Figure 4.24: Effective BESS evolution for April

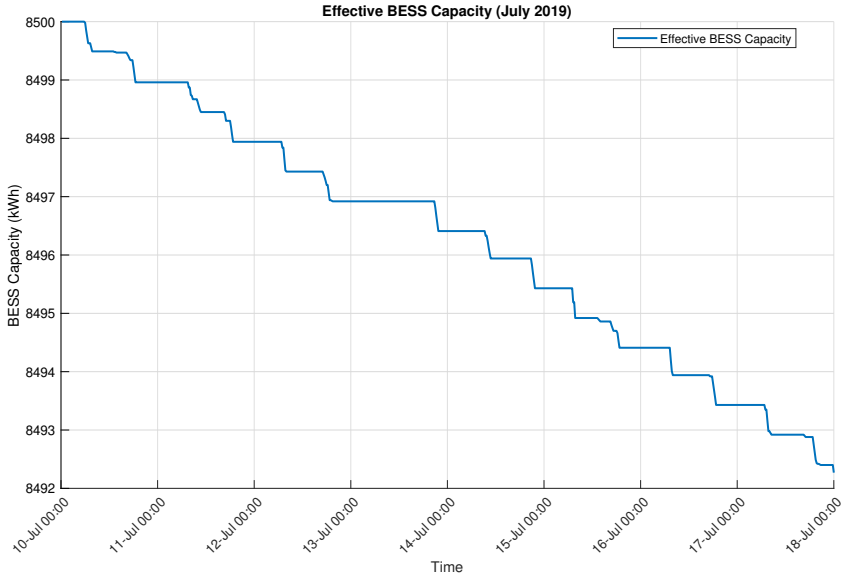

Figure 4.25: Effective BESS evolution for July

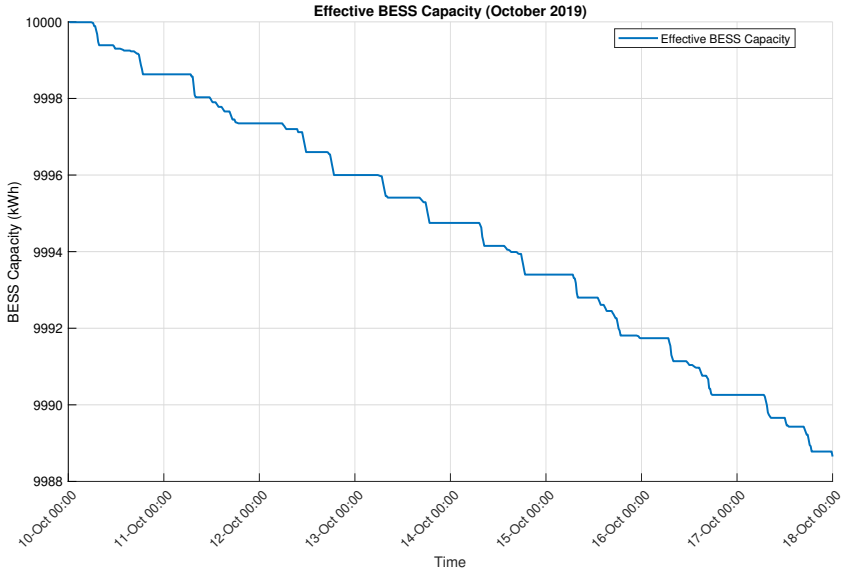

Figure 4.26: Effective BESS evolution for October

Table 4.5 shows the BESS degradation results. Here, it is seen that the darker months of January and October have the largest BESS capacity, with 12 MWh and 10 MWh, respectively. The sunnier months of April and July have the smaller BESS capacities, with 7 MWh and 8.5 MWh, respectively. This shows that the differences in PV generation and overall flight charging demand can have BESS sizing differences of up to 5 MWh of capacity.
When looking at the loss in %, each simulation has a similar loss, as the discharging cycles are similar in number. Finally, the BESS's lifetime is predicted by marking an end of life capacity which corresponds to 70% of the original capacity. With this, it can be seen that the BESS would have to be replaced each 5-6 years. It is important to note that the overall degradation was derived with a simple model. In real life, BESS degradation is a highly complex subject where many factors influence the degradation rate.

Table 4.5: BESS Degradation Results

Month	BESS Capacity (MWh)	Capacity Loss (kWh)	Loss to original(%)	Lifetime [y]
January	12	12.63	0.11	5.06
April	7	7.73	0.11	5.08
July	8.5	8.09	0.095	6.06
October	10	11.35	0.11	5.23

4.6. Baseline Case

To measure the impact that optimization has on the system, a baseline case was set up for the January scenario, as that proved to be the worst scenario of the simulations. Here, the BESS size is set to the previously found 12 MWh, the C-rates to charge the aircraft are set to 1C to remove their optimization. Additionally, the objective function is replaced with a dummy objective that lets the model be solved without minimizing anything from the model. After the solve, all relevant variables and parameters are extracted to get the same outputs that were previously present. In Table 4.6 it is seen that the total delay time imposed in the baseline case is 72 hours, an increase of almost 58 hours compared to the optimized case. With this increase, the average delay time jumps from 44 minutes to 105 minutes. It is important to note that the delays imposed in the FSGA category all stem from very short original turnaround times and are minimally extended to deliver the required energy. Furthermore, a total of 19 flights are canceled, with 7 in the CA category and 12 in the CA2 category. In total, 19 of the 69 total flights were canceled, which corresponds to a rate of 27.5%. Of the 50 remaining flights, 41 of them were canceled meaning that 82% of non-canceled flights are delayed.

Table 4.6: Flight results for January

Category	Count	Delayed Flights	Delay Time (min)	Average Delay (min)	Canceled Flights
FSGA	15	6	103.7	17.3	0
BA	0	0	0	0	0
CA	31	24	3104	129.3	7
CA2	23	11	1091.2	99.2	12
Total	69	41	4298.9	104.9	19

Figure 4.27 shows the power curves for the base case. Here, it can be seen that the grid is constantly importing at its full capacity of 3.5 MW throughout the simulation. The charge powers, even with many delays and cancellations, still have frequent peaks in the magnitude of 15 MW, with spikes up to 20-22 MW. Lastly, the BESS frequently discharges, only having a longer charging period during January 14. It reaches its maximum discharge power of 24 MW once.

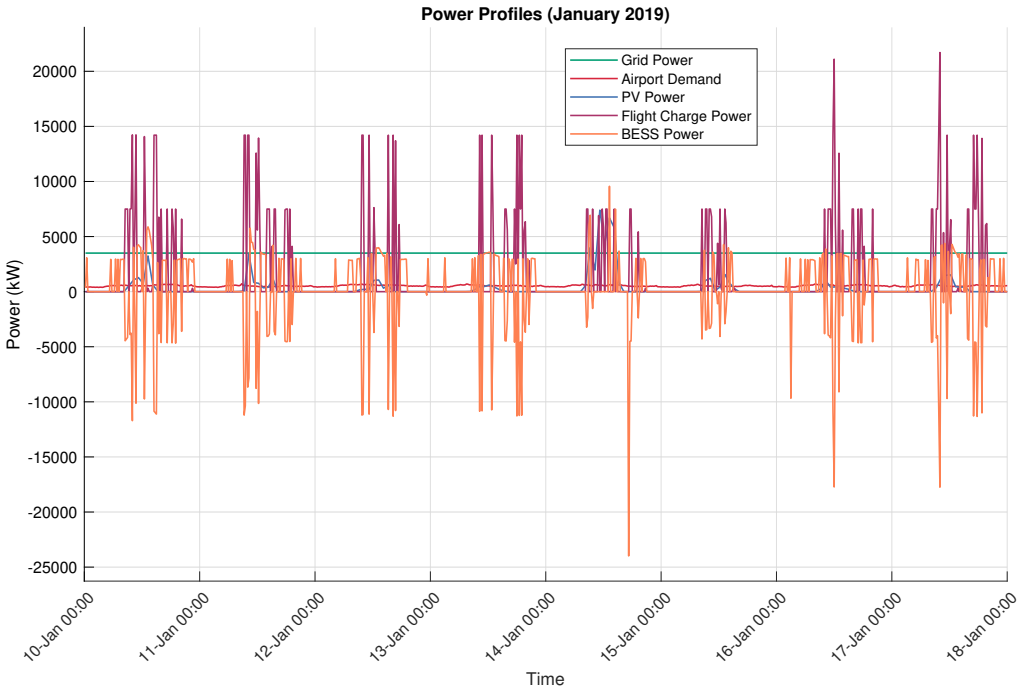

Figure 4.27: Power curves for base case January

4.7. Simulation Costs

The final section will evaluate the total cost of operations for each scenario, including grid costs, PV curtailment costs, delay costs, cancellation costs, and BESS degradation costs. These are determined by the turnaround times, power flows, SoC, and degradation trends discussed in Sections (4.2) through (4.6). Additionally, the sizing of the BESS itself will be discussed, as it would be a new investment made by RTHA.

Table 4.7 shows an overview of each cost associated to each simulation period. Here, it shows that the sunnier months of April and July have operational costs that earn money for the airport due to a lower charging demand and higher PV availability. In January and October, the operational costs range from 16300-168600 euro, where the latter is due to high grid reliance, low PV availability, long delays, and three cancellations. BESS capacities range from 7 MWh to 12 MWh, which is a difference of up to one million euros in investment cost. Lastly, when comparing the baseline case to the optimized January case, it becomes very clear that optimization has made significant improvements to the costs. In the baseline case, the grid is constantly importing, making for costly grid usage. With no penalties for delays or cancellations and a fixed C-rate, the costs increased by approximately 600%. With optimization, almost half a million in operational costs can be saved. Finally, with no incentive to ideally utilize the PV power, more of its energy has not been used. Figures (4.28) and (4.29) provide a graphical overview regarding the costs of the scenarios.

Table 4.7: Cost breakdown of simulations

	January	**April**	**July**	**October**	**Baseline**
C_{grid}(€)	88281.81	-22576	-21059.4	12985.22	145038.7
$C_{\text{BESS,deg}}$(€)	2526.07	1585.28	1545.95	2282.87	2278.57
C_{delay}(€)	15020.54	985.01	85.344	1056.13	90592.66
C_{cancel}(€)	62790	0	0	0	397670
$C_{\text{PV,curt}}$(€)	0	47.22	72	8.97	18481.35
C_{total}(€)	168618.42	-20005.7	-19356.1	16333.19	654061.3
Q_{BESS}(MWh)	12	7	8.5	10	12
$C_{\text{BESS,inv}}$(M€)	2.4	1.4	1.7	2	2.4

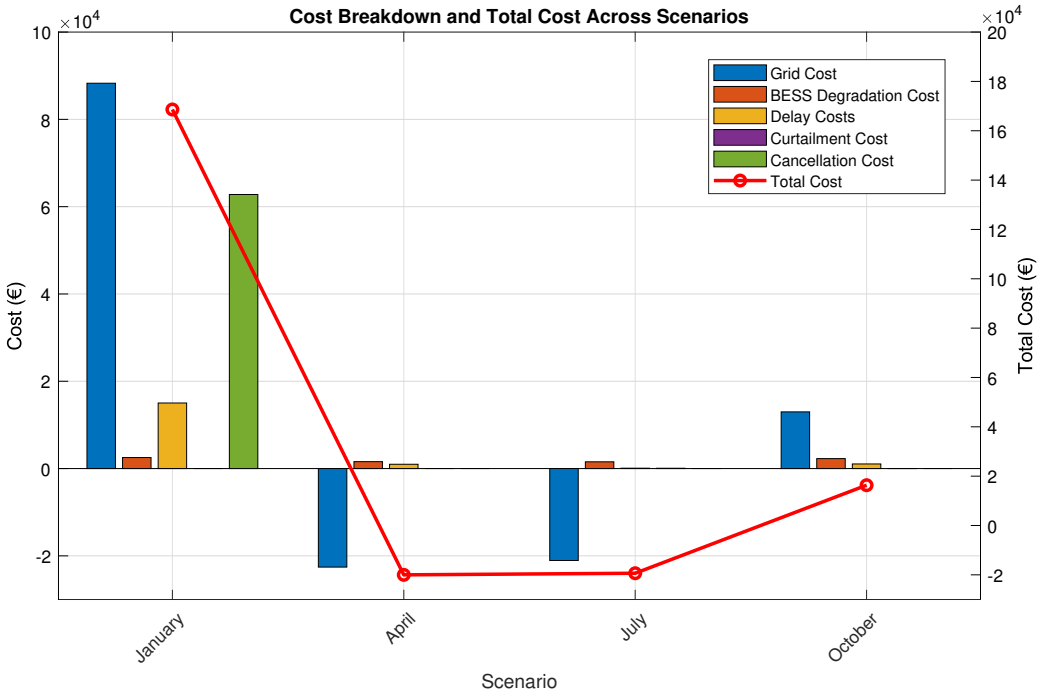

Figure 4.28: Cost breakdown per scenario

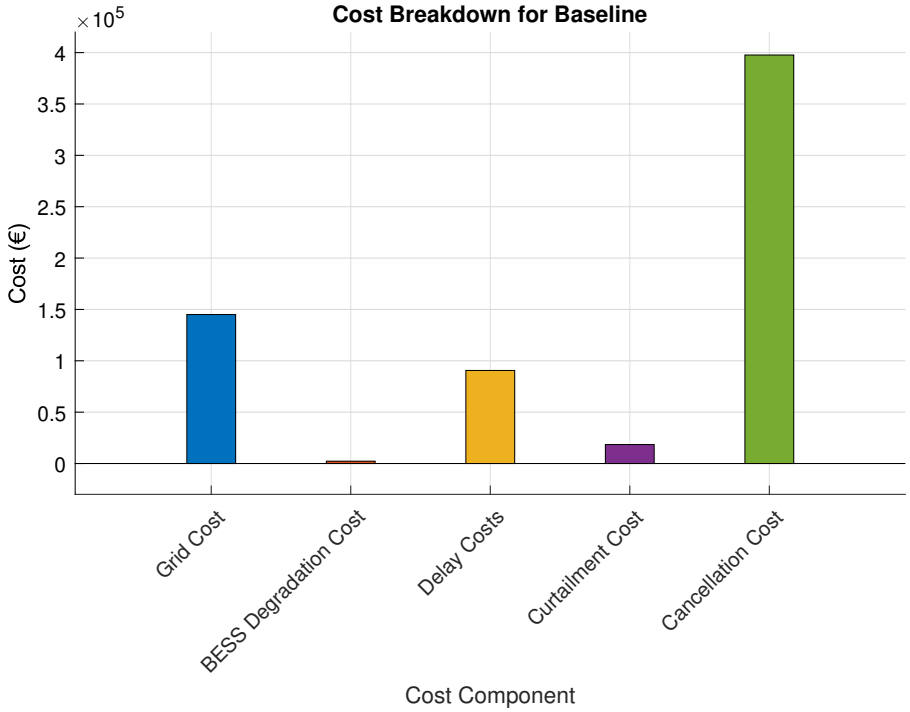

Figure 4.29: Cost breakdown of baseline case

5

Sensitivity Analysis

In this chapter, a sensitivity analysis is conducted to evaluate the impact of parameter variations on the model's performance during January, the worst performing week, to understand the factors that affect cost and flight performance. Here, grid parameters for import and export, turnaround time extensions, higher BESS capacity, and different cost weights will be changed to measure their impact on the results and will be compared to the original results for January. In each simulation, only one parameter will be adjusted to isolate their impact on the results. Additionally, the BESS size is fixed to the original value of 12 MWh.

5.1. Grid Parameters

First, the grid power limits of the model will be adjusted for both import and export values. The original grid limits are 3.5 MW for import and 7.5 MW for export. For import, a simulation will be done with a 2 MW import limit and a 5 MW limit. For export, the simulations will be conducted with limits of 5 MW and 10 MW.

2 MW Import

When the grid import limit is decreased, it is seen that a total of 11 flights need to be canceled during the week, in addition to 15 flights that need average delays of 51 minutes. From Figure 5.1, the grid is almost always importing power, either to help with the charging demand or to charge the BESS. The latter happens less frequently, seen by a limited amount of charging power delivered to the BESS itself. The combination of lower grid import with large BESS size and little PV power, makes the BESS less effective in aiding the system as it receives less energy during the simulation.

Table 5.1: Flight results for January with 2 MW import limit.

Category	Count	Delayed Flights	Delay Time (min)	Average Delay (min)	Canceled Flights
FSGA	15	6	61.2	10.2	0
BA	0	0	0	0	0
CA	31	3	194.2	64.7	0
CA2	23	6	512.2	85.37	11
Total	69	15	767.6	51.17	11

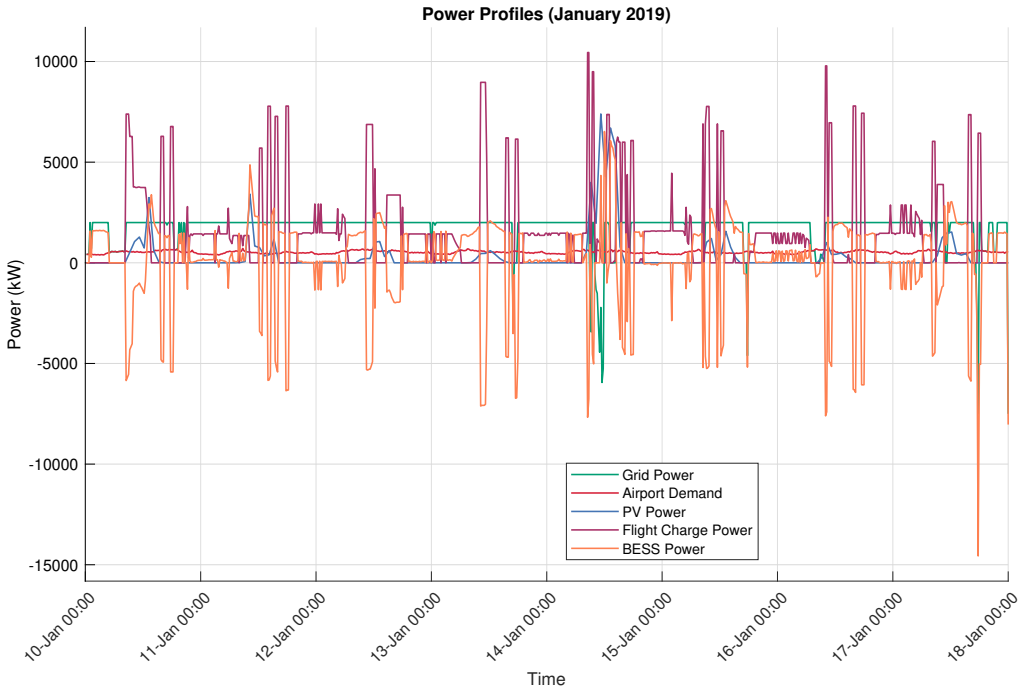

Figure 5.1: Power curves for 2 MW import

5 MW Import

When the grid import limit is increased to 5 MW, the system performs better for the flight schedule. A more reliable amount of power is available at all time for the system. In this week, only one flight was canceled, compared to the three in the original January case. The total delay time is increased by 35 minutes, while there are two flights less that have been delayed. This is due to the system being able to charge the originally canceled flights, which probably needed an extension of the turnaround time to fulfill the charging needs. The charging peaks peak at values of 20 MW, while the grid powers are now switching more between importing and exporting, which in turn aids in charging the BESS when there is lower demand.

Table 5.2: Flight results for January with 5 MW import limit.

Category	Count	Delayed Flights	Delay Time (min)	Average Delay (min)	Canceled Flights
FSGA	15	6	61.2	10.2	0
BA	0	0	0	0	0
CA	31	2	9.4	4.7	0
CA2	23	10	809.4	80.9	1
Total	69	18	880	48.9	1

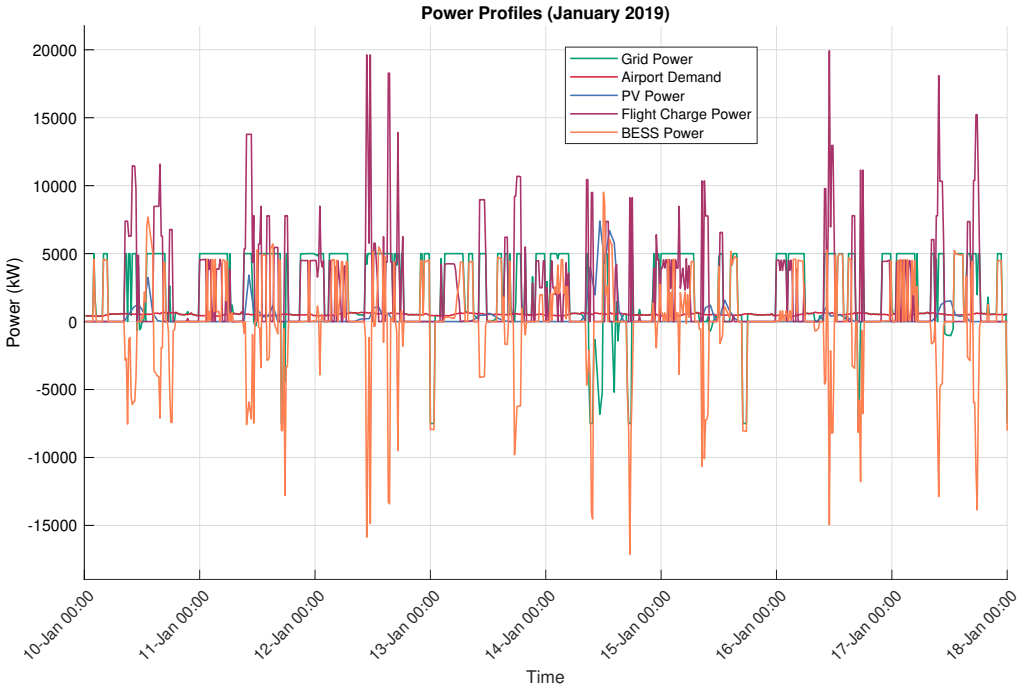

Figure 5.2: Power curves for 5 MW import

5 MW Export

When the export limit is adjusted, it changes the amount of excess energy that can be sold back to the grid. If this is lowered, it can force the system to store more energy in the BESS or to adjust the flight schedule by adding delay times to balance the energy demand and supply. Exporting energy is the only possibility for the system to make money and could force the system to lower other costs, such as cancellations and delays. In turn, it would spread the delays across multiple flights, reflecting the higher delay times compared to the original case. The same amount of flights are delayed as in the original scenario, albeit with a higher average delay.

Table 5.3: Flight results for January with 5 MW export limit.

Category	Count	Delayed Flights	Delay Time (min)	Average Delay (min)	Canceled Flights
FSGA	15	6	61.2	10.2	0
BA	0	0	0	0	0
CA	31	4	103.6	25.9	0
CA2	23	10	815	81.5	3
Total	69	20	979.8	49	3

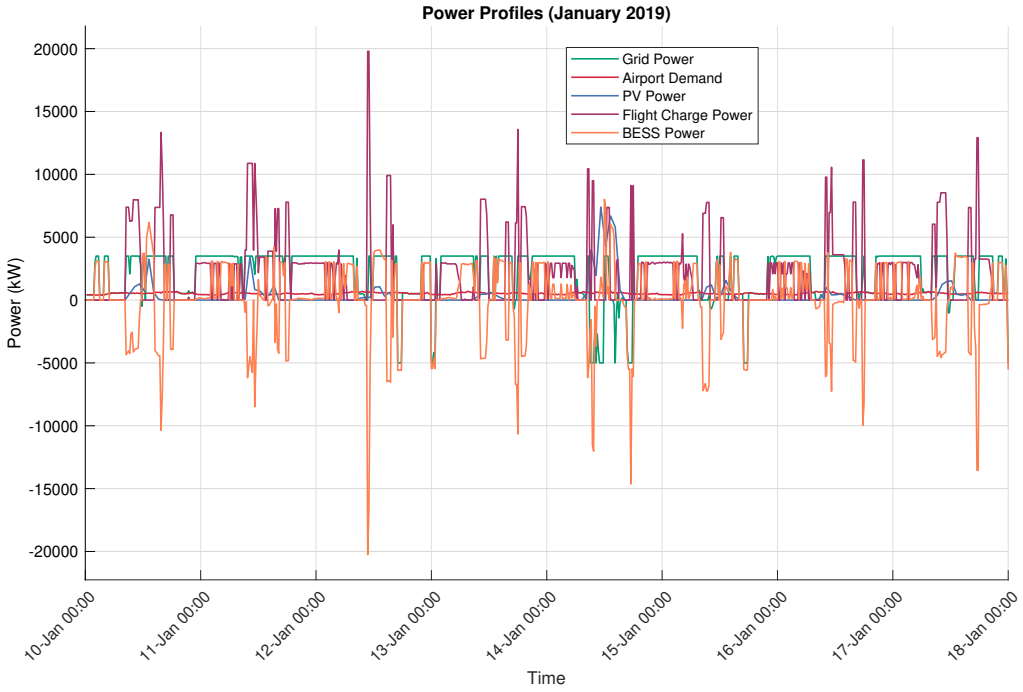

Figure 5.3: Power curves for 5 MW export

10 MW Export

When the export limit is increased, the system has more options to offload excess energy. This reduces the BESS usage or peak demands, as it exports energy less frequently than the 5 MW export scenario, where it would have to use two time steps to export the energy from one time step in the 10 MW scenario. This might have fixed a bottleneck in scheduling, allowing one flight less to be canceled while lowering the total delay time by almost 30 minutes in comparison to the original January case.

Table 5.4: Flight results for January with 10 MW export limit.

Category	Count	Delayed Flights	Delay Time (min)	Average Delay (min)	Canceled Flights
FSGA	15	6	61.2	10.2	0
BA	0	0	0	0	0
CA	31	4	43.6	10.9	0
CA2	23	10	748.2	68	2
Total	69	21	853	40.62	2

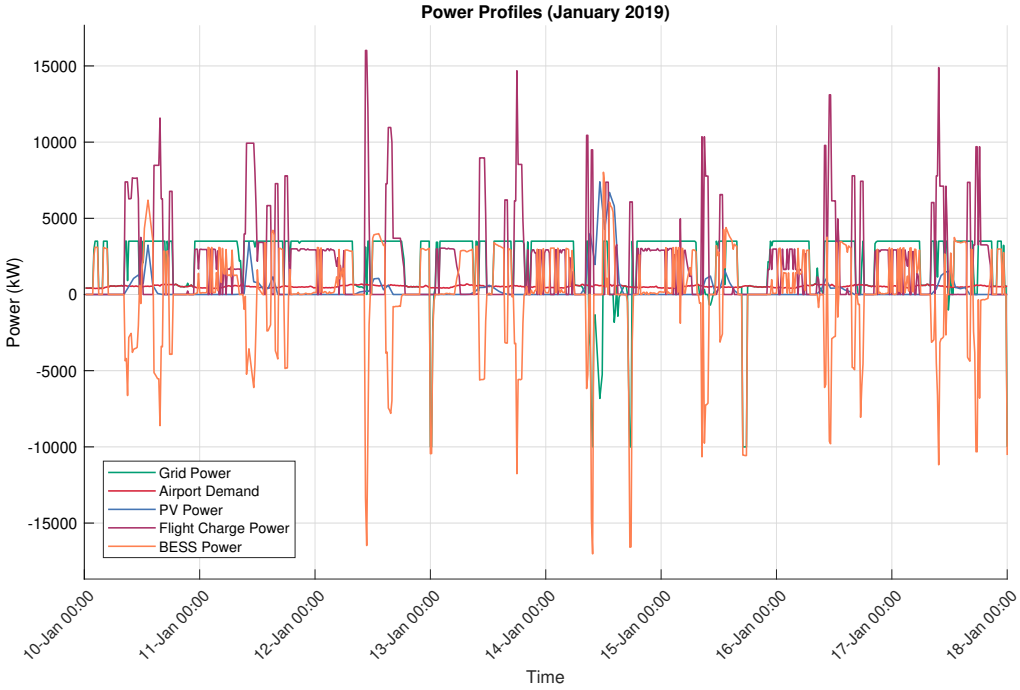

Figure 5.4: Power curves for 10 MW export

5.2. BESS Size

To evaluate the effect of increasing the energy storage capacity, the original BESS size was increased from 12 MWh to 13 MWh. A decrease of the BESS was not considered, as the aforementioned capacity of 12 MWh was already determined to just be sufficient to aid the demand. This increase resulted in large improvements to the system's ability to fulfill the flight schedule. Here, the number of canceled flights decreased by one, while the total delay time was reduced by 5 hours compared to the original January case. With additional BESS capacity, the system can store more energy provided by either the PV park or the grid imports during periods of lower demand. This extra stored energy aided the system during high charging demand and lowered scheduling problems that would have led to delay times or more cancellations in the original case. A larger BESS can be a critical factor to optimize the flight operations.

Table 5.5: Flight results for January with 1 MWh additional BESS size.

Category	Count	Delayed Flights	Delay Time (min)	Average Delay (min)	Canceled Flights
FSGA	15	6	61.2	10.2	0
BA	0	0	0	0	0
CA	31	2	36	18	0
CA2	23	10	489	48.9	2
Total	69	18	586.2	30.57	2

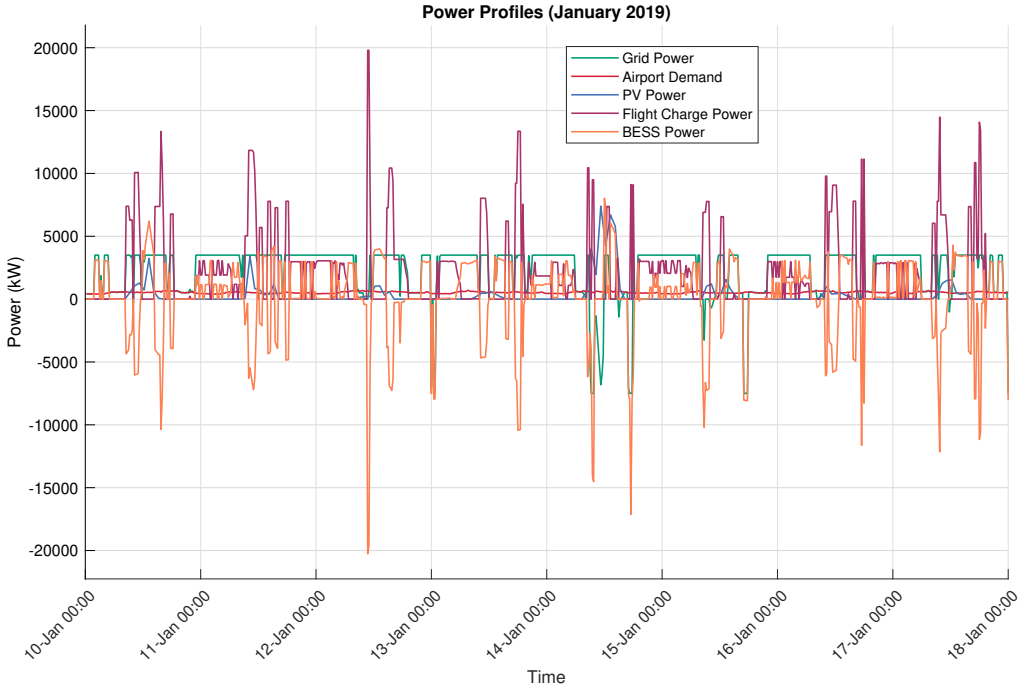

Figure 5.5: Power curves for 13 MWh BESS

5.3. Turnaround shortened and prolonged

Lastly, the impact of adjusting the original turnaround times was measured. First, a decrease of 15 minutes was applied, which can account for taxiing, and afterwards an increase of 15 minutes was applied to add some flexibility to the scheduling.

15 minute decrease

In the case where 15 minutes were removed from the turnaround time, it is seen from the results that it closely matches the original case. There are three canceled flights, and the delay time is 12 minutes less. This suggests that the system maintains sufficient flexibility with a shorter turnaround time, which is good for tighter flight schedules. The existing BESS and grid limits can support the shorter windows, which prevent significant changes to the flight schedule. In conclusion, it can handle reductions in turnaround times without losing operational efficiency,

Table 5.6: Flight results for January with 15 minutes less turnaround time.

Category	Count	Delayed Flights	Delay Time (min)	Average Delay (min)	Canceled Flights
FSGA	15	6	61.2	10.2	0
BA	0	0	0	0	0
CA	31	12	168.2	14	0
CA2	23	11	638.6	58	3
Total	69	29	868	29.93	3

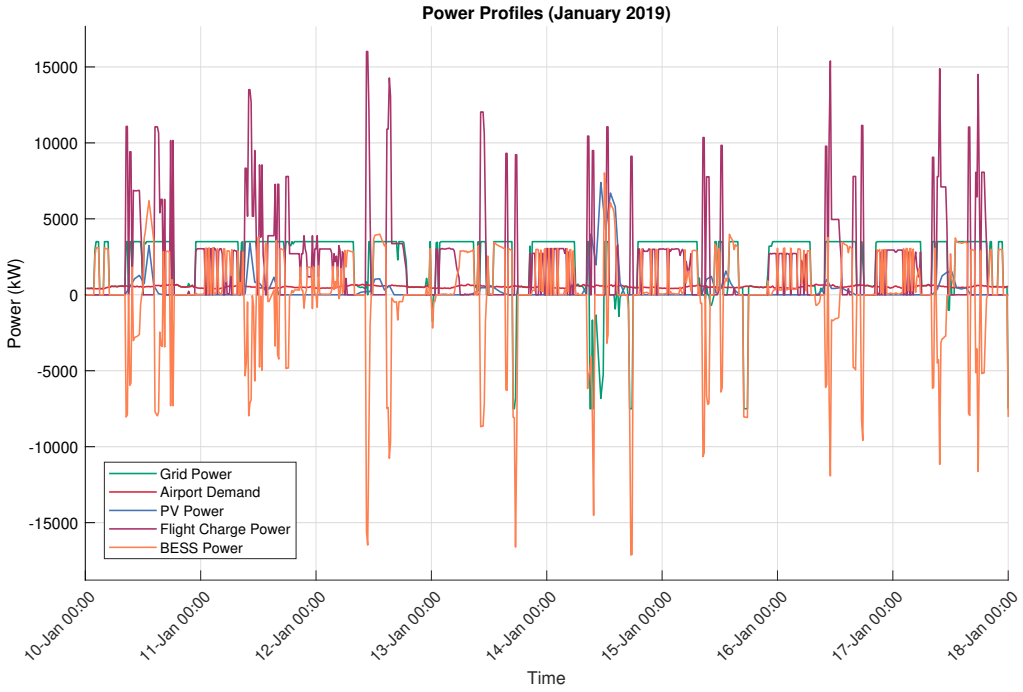

Figure 5.6: Power curves for -15 min turnaround time

15 minute increase

When the turnaround time was increased by 15 minutes, the total delay time jumped up by roughly 4 hours compared to the original scenario. With extended turnaround windows, the model would hold off charging which increased delays across flights. With the current weights, the system did not have enough incentive to keep the delay times low, as it had more time to charge the aircraft without adding more cancellations.

Table 5.7: Flight results for January with 15 minutes more turnaround time.

Category	Count	Delayed Flights	Delay Time (min)	Average Delay (min)	Canceled Flights
FSGA	15	1	1.8	1.8	0
BA	0	0	0	0	0
CA	31	1	101.8	101.8	0
CA2	23	9	1102	122.4	3
Total	69	11	1205.6	109.6	3

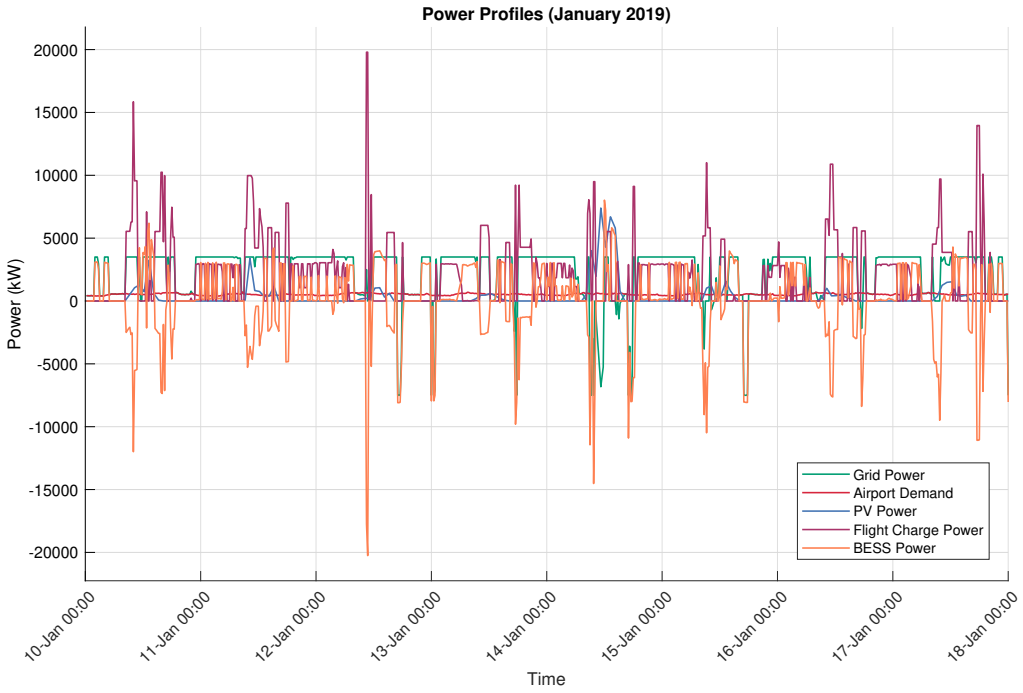

Figure 5.7: Power curves for +15 min turnaround time

5.4. Cost Overview

To conclude, an overview of the associated objective costs for each scenario is found in Table 5.8 and a visual representation is given in Figure 5.8. The largest factor in cost is the cancellation costs. For the case where only 2 MW of import power was present, it increased the total cost exponentially where costs ramped up to 230 000 euro. In each scenario, the full PV power that was generated was used by the system, leading to no costs for curtailment. The grid costs ranged from 70 000 - 91 000 euro per week. BESS degradation was relatively the same for all scenarios, except for the 2 MW import one, where there was less power available to charge the BESS, decreasing its ability to discharge its energy during the simulation. The lowest overall cost came from the scenario with 5 MW import power, where the cost compared to the original case was lowered by almost 40 000 euro. This highlights the importance of a larger grid connection and bigger BESS capacity in the functioning of a flight schedule with electric aircraft. However, extra thought regarding the turnaround adjustments needs to be considered. For example, adding a higher delay penalty weight to ensure the model does not extend the turnaround times to make money.

Table 5.8: Cost breakdown sensitivity

	2 MW Import	**5 MW Import**	**5 MW Export**	**10 MW Export**	**13 MWh BESS**	**-15 min Turnaround**	**+15 min Turnaround**
C_{grid}(€)	70893.82	91082.33	88151.21	90430.28	90665.19	88335.48	87651.12
$C_{\text{BESS,deg}}$(€)	1858.367	2482.3	2317.358	2448.23	2550.03	2434.68	2341.1
C_{delay}(€)	13647.93	15646.4	17420.84	15166.34	10422	15433	21435.57
C_{cancel}(€)	230230	20930	62790	41860	41860	62790	62790
$C_{\text{PV,curt}}$(€)	0	0	0	0	0	0	0
C_{total}(€)	316630.1	130141	170679.4	149904.8	145497.86	168993.2	174217.8

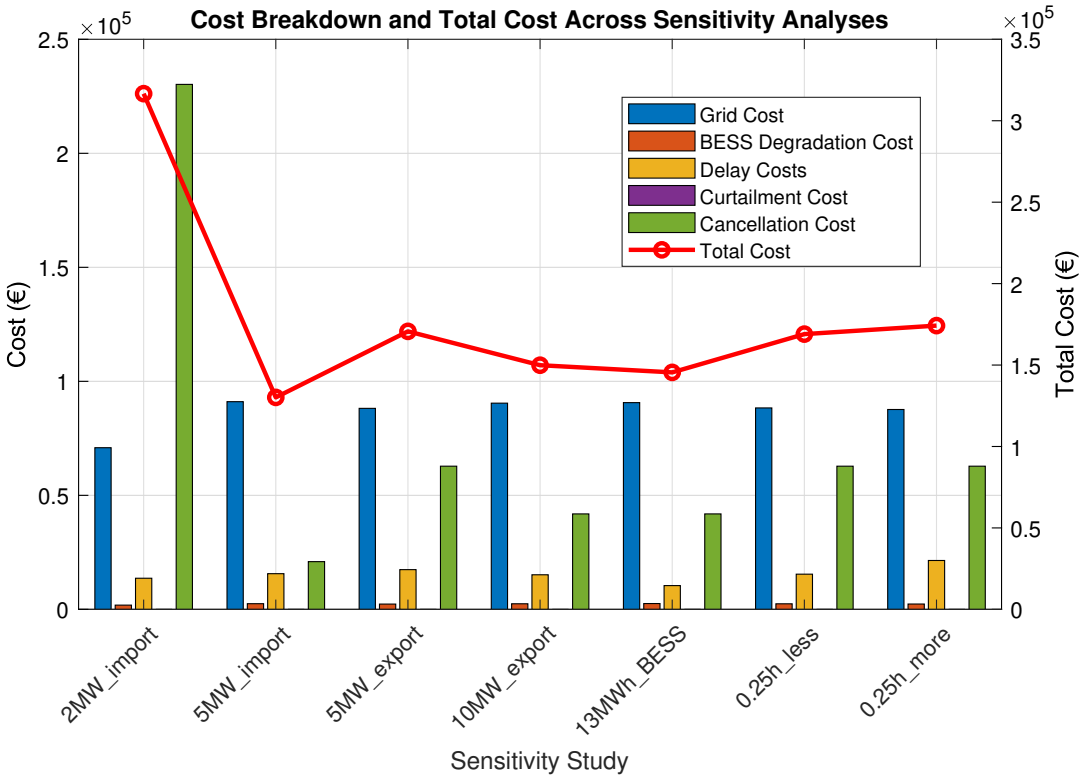

Figure 5.8: Cost breakdown per study done

5.5. Case Studies

To finish the sensitivity analysis, two case studies were done to see the impact on the system if there would be no delays and cancellations. The two cases are one where there is no BESS available, to measure the grid expansion needed to fulfill the flight schedule. Then, the same case is simulated, but with the BESS in the system to find a balance between grid and battery to fulfill the flight schedule.

Grid Only

If we want the system to run without imposing any delays or cancellations, the grid should be able to provide power peaks of over 47 MW at the same time, as seen in Figure 5.9. Even if the full 10 MVA connection is utilized, a grid upgrade of 37 MVA would still be needed to adhere to the flight schedule.

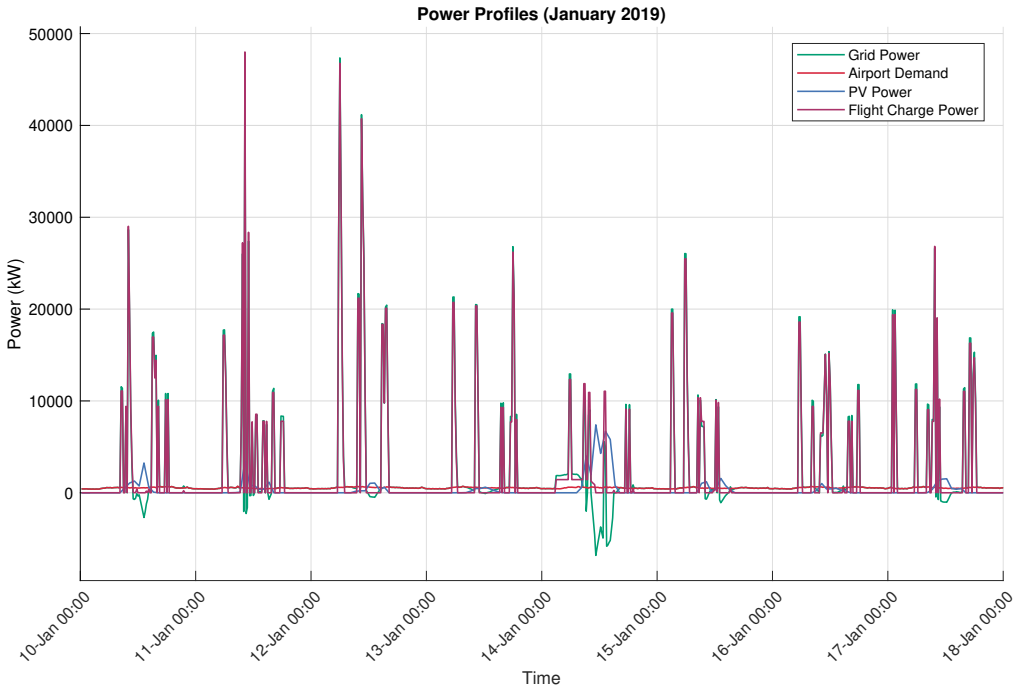

Figure 5.9: Power curves for grid only and no delays January

Grid and BESS

In the second case study a trade-off between grid upgrade cost and BESS investment cost is done to determine a long-term strategy. Now, the objective function gets two new costs, $C_{\text{grid,upgrade}}$ and $C_{\text{BESS,invest}}$. To account for the large prices of these two costs, they will be estimated to their weekly share during the simulation. For the BESS, a lifetime of 5 years is taken, roughly based on the results from chapter 4. Therefore, the cost function for BESS investment is as follows:

$$C_{\text{BESS,invest}} = (C_{1\text{kWh}} \cdot Q_{\text{BESS}})/260 \tag{5.1}$$

Where the factor 260 is 5 years in weeks.

To estimate how much a grid upgrade costs, tariffs from the energy supplier Stedin are used [24]. In the document, there are multiple price points to invest in a new connection to the grid, and its power rating. Unfortunately, anything above 10 MVA is based on project specifics and has no cost associated with it. Because of this, a rough linear approximation will be used to determine the cost of upgrading the grid. Figure 5.11 depicts the prices alongside their power ratings and the trendline that estimates them.

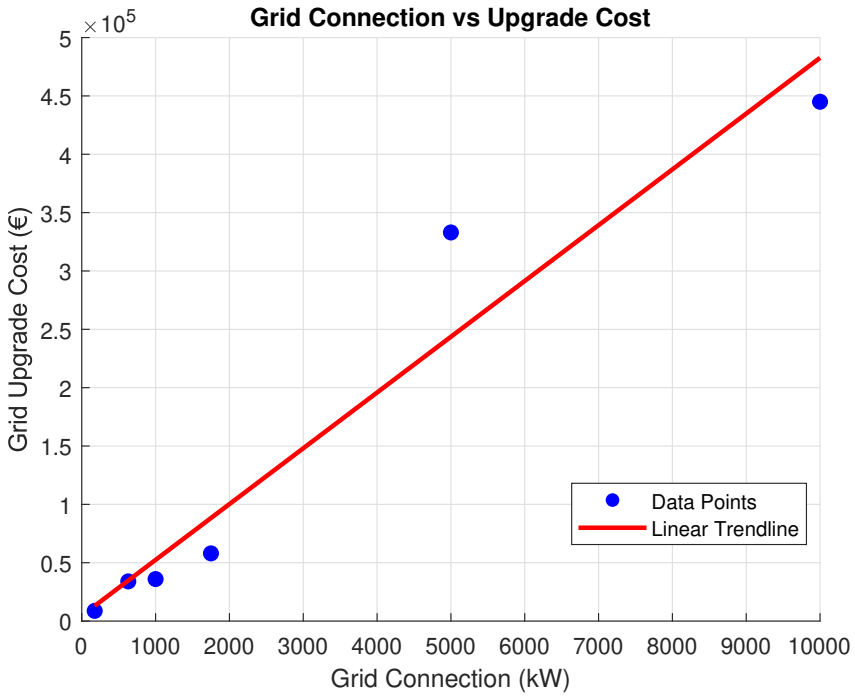

Figure 5.10: Grid upgrade cost approximation

From this trendline, an approximation of the grid cost can be found:

$$C_{\text{grid,upgrade}} = 47.718 \cdot P^{\text{max}}_{\text{grid,import}}(\text{kW}) + 4391.2 \tag{5.2}$$

The existing connection is rated for 10 MVA, but only 3.5 MVA is available for use. Therefore, everything higher than 3.5 MVA should be included in the upgrade cost. Furthermore, to factor the weekly price share of this upgrade, a 50-year lifespan is taken for the grid connection [25]. With these, the final grid upgrade cost function is as follows:

$$C_{\text{grid,upgrade}} = (47.718 \cdot (P^{\text{max}}_{\text{grid,import}}(\text{kW}) - 3500) + 4391.2)/2600 \tag{5.3}$$

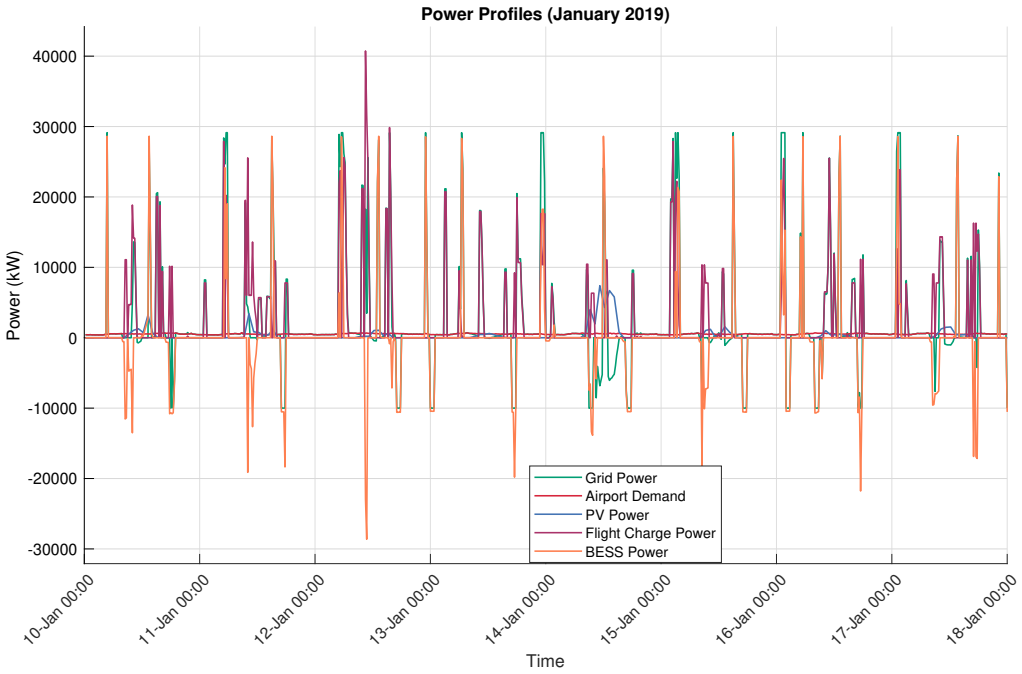

Figure 5.11: Power curves for BESS and grid for no delays in January.

From the simulation, it is found that the grid would need a new power rating of just over 29 MW in combination with a BESS size of 14.3 MWh to fulfill the flight schedule without delays and cancellations. Important to note is that the maximum export power was set to 10 MW. If it was kept unbounded to follow the import limit, the solver would keep increasing the BESS size to allow for higher export limits that make up some of the cost.

6

Conclusion

This study optimized the energy management and flight scheduling for electric aviation at Rotterdam The Hague Airport considering a BESS and PV generation across January, April, July, and October 2019. Seasonal delays averaged 2 minutes in July and peaked at 45 minutes in January, being highly dependent on PV availability and flight charging demand. Only in January were there three flights that needed to be canceled due to high energy needs. Power dynamics showed that April and July reduced the reliance of grid and BESS powers, while January and October showed that higher grid and BESS powers were necessary to fulfill operations due to lower PV generation.

The BESS SoC cycling varied from month to month, all utilizing the full 10%-100% range while using vastly different cycling patterns. Scenarios with lower PV availability and high charge power demands had trouble charging the BESS during daytime operations. Degradation of the BESS after a one-week operation peaked at roughly 0.11% in winter, spring, and fall, which is linked to the high discharge rates and frequent cycling of the battery. Overall operational costs varied greatly, with totals ranging from 168618 euro in January operational costs per week due to cancellations, to earning upward of 20000 euro per week in April and July by smartly utilizing available energy and extra PV power. Differences of up to one million euro in BESS sizing cost are found, with the found capacities ranging from 7 MWh to 12 MWh.
The found optimized BESS capacity is effective in managing large charging peaks, even under conditions of limited PV availability and imposed delay times. However, it faces challenges during winter, when the high number of CA and CA2 flights within short time windows places excessive demand on the system. This highlights the critical importance of additional energy strategies, such as grid infrastructure upgrades, in mitigating costs and compensating for seasonal PV variability and limited grid capacity.

When comparing the flight distribution over the simulated weeks with the averages found in chapter 2, it can be seen that the chosen weeks align with the expectations from the analysis. Additionally, it has shown that the time difference between arrivals for CA and CA2 flights is an important parameter that has a large impact on the delay time and number of canceled flights.
Finally, the baseline case for January showed that optimization can reduce operational costs by up to half a million euro per week.

The sensitivity analysis revealed that adjusting import limits has a significant impact on the system. With a lower power availability, more flights had to be canceled, while a larger power limit lowered delays and had two flight cancellations less.
It showed that export limits impacts system performance, where a lower limit increased delays due to utilizing more time step to export this energy, thus straining BESS and grid resources. An increase in export power showed a decrease in delays and cancellations by one, showing improved energy management.
Increasing the BESS size by 1 MWh reduced cancellations by one and delays by up to 5 hours for the

week, which highlights the importance of extra energy storage to mitigate flight scheduling constraints. Lastly, varying the turnaround time shows that the model works well with stricter turnaround time windows, but was more willing to impose delays with extended turnaround time applications. Here, the delays increased by up to 4 hours for the week's duration.
Key takeaways are that energy storage and grid upgrades are key components for reliability in operations, and should be one of the highest priorities for the future.

Future Work

Future work should extend the model to run for a monthly or seasonal scope to capture degradation of the BESS fully while integrating real-life PV data sourced from the system. The 12 MWh BESS that was found for January was not applied to the other months as the objective was to look at the pessimistic cases. However, with a larger BESS size during the other periods, the delays could be lowered even further, and the rate of degradation would be slowed, allowing a longer lifetime for the BESS. Optimizing charger numbers could determine an effective cost which balances the capital investment versus operational savings. Exploring nonlinear models might finetune results for the workings of the BESS, as it is better for modeling battery degradation while also being more accurate in determining charging powers during the CPCV charging profiles. This is in line with the idea to upgrade the grid capacity at RTHA in the upcoming years. An unexplored area of the thesis is charger optimization. By considering the number of chargers in the system, a more realistic charging power can be estimated considering the availability of chargers. Investigating strategies that shift around flights could potentially lower the overall delay time and BESS capacity needed for the project. Additionally, an insight that takes into account passenger throughput can be analyzed to more closely match real-world figures. This would increase the number of commercial electric airplanes, causing the system to be more affected by increased demand. Lastly, the impact of grid upgrades and BESS investments can be refined further with more accurate lifetimes and pricing.

References

[1] EUROCONTROL. *EUROCONTROL Aviation Outlook 2050*. 2022.

[2] Reynard de Vries et al. “A New Perspective on Battery-Electric Aviation, Part II: Conceptual Design of a 90-Seater”. In: *AIAA SCITECH 2024 Forum*. DOI: 10.2514/6.2024-1490. eprint: https://arc.aiaa.org/doi/pdf/10.2514/6.2024-1490. URL: https://arc.aiaa.org/doi/abs/10.2514/6.2024-1490.

[3] Boya Hou et al. “Impact of Aviation Electrification on Airports: Flight Scheduling and Charging”. In: *SSRN Electronic Journal* (Jan. 2022). DOI: 10.2139/ssrn.4131207.

[4] Mihaela Mitici, Madalena Pereira, and Fabrizio Oliviero. “Electric flight scheduling with battery-charging and battery-swapping opportunities”. In: *EURO Journal on Transportation and Logistics* 11 (2022), p. 100074. ISSN: 2192-4376. DOI: https://doi.org/10.1016/j.ejtl.2022.100074. URL: https://www.sciencedirect.com/science/article/pii/S2192437622000036.

[5] Patrik Ollas et al. “Evaluating the role of solar photovoltaic and battery storage in supporting electric aviation and vehicle infrastructure at Visby Airport”. In: *Applied Energy* 352 (2023), p. 121946. ISSN: 0306-2619. DOI: https://doi.org/10.1016/j.apenergy.2023.121946. URL: https://www.sciencedirect.com/science/article/pii/S0306261923013107.

[6] Algot Laurell. *Charging Infrastructure for Battery Electric Aircraft: A Simulation Study*. 2023.

[7] Finn Vehlhaber and Mauro Salazar. “Electric Aircraft Assignment, Routing, and Charge Scheduling Considering the Availability of Renewable Energy”. In: *IEEE Control Systems Letters* 7 (2023), pp. 3669–3674. ISSN: 2475-1456. DOI: 10.1109/lcsys.2023.3339998. URL: http://dx.doi.org/10.1109/lcsys.2023.3339998.

[8] Simon van Oosterom and Mihaela Mitici. “Optimizing the battery charging and swapping infrastructure for electric short-haul aircraft—The case of electric flight in Norway”. In: *Transportation Research Part C: Emerging Technologies* 155 (2023), p. 104313. ISSN: 0968-090X. DOI: https://doi.org/10.1016/j.trc.2023.104313. URL: https://www.sciencedirect.com/science/article/pii/S0968090X23003029.

[9] Markus Meindl et al. “Operating Strategies for a Regional Airport To Challenge Future Hybrid-Electric Aircraft Systems”. In: *AIAA AVIATION FORUM AND ASCEND 2024*. DOI: 10.2514/6.2024-4184. eprint: https://arc.aiaa.org/doi/pdf/10.2514/6.2024-4184. URL: https://arc.aiaa.org/doi/abs/10.2514/6.2024-4184.

[10] Alternergy. *C-Rates for Commercial Battery Storage Systems*. Apr. 5, 2025. URL: https://www.alternergy.co.uk/blog/post/battery-c-rates-for-commercial-battery-storage-systems (visited on 06/12/2025).

[11] PHOTOVOLTAIC GEOGRAPHICAL INFORMATION SYSTEM. *PHOTOVOLTAIC GEOGRAPHICAL INFORMATION SYSTEM*. URL: https://re.jrc.ec.europa.eu/pvg_tools/en/ (visited on 05/14/2025).

[12] ENTSO-E. *About ENTSO-E*. URL: https://www.entsoe.eu/about/ (visited on 05/14/2025).

[13] ENTSO-E. *ENTSO-E Transparency Platform*. URL: https://newtransparency.entsoe.eu/ (visited on 05/14/2025).

[14] Pipistrel. *Velis Electro*. URL: https://www.pipistrel-aircraft.com/products/velis-electro/ (visited on 05/14/2025).

[15] Yawen Liang et al. “Charging Demand Prediction: Small All-Electric Aircraft and Electric Vertical Takeoff and Landing Aircraft”. In: *IEEE Transactions on Transportation Electrification* 11.1 (2025), pp. 2732–2747. DOI: 10.1109/TTE.2024.3427841.

[16] Door Redactie Piloot en Vliegtuig. “Maeve Aerospace toont aangepast ontwerp Maeve-01”. In: *Piloot en Vliegtuig* (Apr. 16, 2023). URL: https://www.pilootenvliegtuig.nl/nieuws/maeve-aerospace-toont-aangepast-ontwerp-maeve-01/ (visited on 05/14/2025).

[17] Elysian. *Elysian Aircraft*. URL: https://www.elysianaircraft.com/ (visited on 05/14/2025).

[18] xAI. *Grok: An Artificial Intelligence Assistant*. Used for determining aircraft types and passenger counts. Accessed via https://grok.com. 2025. URL: https://grok.com.

[19] Oktavia Catsaros. “Lithium-Ion Battery Pack Prices See Largest Drop Since 2017, Falling to $115 per Kilowatt-Hour : BloombergNEF$”. In: *BloombergNEF* (Dec. 10, 2024). URL: https://about.bnef.com/blog/lithium-ion-battery-pack-prices-see-largest-drop-since-2017-falling-to-115-per-kilowatt-hour-bloombergnef/ (visited on 05/14/2025).

[20] Tesla. *Tesla Megapack*. URL: https://www.tesla.com/megapack (visited on 05/14/2025).

[21] EUROCONTROL. *Cost of delay*. URL: https://ansperformance.eu/economics/cba/standard-inputs/latest/chapters/cost_of_delay.html (visited on 05/14/2025).

[22] EUROCONTROL. *Cancellation cost*. URL: https://ansperformance.eu/economics/cba/standard-inputs/latest/chapters/cancellation_cost.html (visited on 05/14/2025).

[23] Seoung Jeon et al. “Study on Battery Charging Strategy of Electric Vehicles Considering Battery Capacity”. In: *IEEE Access* PP (June 2021), pp. 1–1. DOI: 10.1109/ACCESS.2021.3090763.

[24] Stedin. *ELEKTRICITEIT TARIEVEN 2025*. URL: https://www.stedin.net/zakelijk/betalingen-en-facturen/tarieven (visited on 06/25/2025).

[25] Szymon Kardaś. *Gridlock: Why Europe’s electricity infrastructure is holding back the green transition*. Oct. 26, 2023. URL: https://ecfr.eu/article/gridlock-why-europes-electricity-infrastructure-is-holding-back-the-green-transition/ (visited on 06/25/2025).